LA-5147

Special Graphites and Carbide-Graphite Composites Developed at LASL

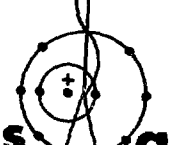

los alamos
scientific laboratory
of the University of California
LOS ALAMOS, NEW MEXICO 87544

UNITED STATES
ATOMIC ENERGY COMMISSION
CONTRACT W-7405-ENG. 36

Printed in the United States of America. Available from
National Technical Information Service
U. S. Department of Commerce
5285 Port Royal Road
Springfield, Virginia 22151
Price: Printed Copy $3.00; Microfiche $0.95

5.45

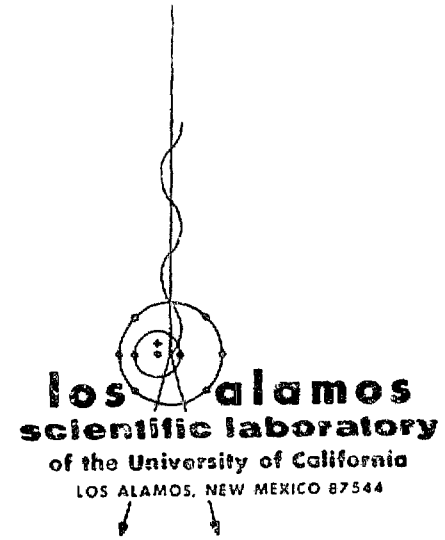

LA-5147
UC-25
ISSUED: April 1973

Special Graphites and Carbide-Graphite Composites Developed at LASL

by

R. E. Riley

This report supersedes LA-3569-MS, LA-3618-MS, LA-3652-MS, and LA-4077.

SPECIAL GRAPHITES AND CARBIDE-GRAPHITE COMPOSITES DEVELOPED AT LASL

by

R. E. Riley

ABSTRACT

Well-characterized materials containing either TaC and graphite or pure graphite were fabricated utilizing powder metallurgy techniques that included hot pressing or hydrostatic pressing and subsequent high-temperature heat treatment. Physical structure and thermal properties were investigated, particularly thermal-stress fracture resistance. We found that well-controlled reproducible materials manifesting an excellent distribution of carbide in the graphite matrix could be fabricated utilizing either technique. Thermal properties were affected significantly by the size and relative amounts of TaC and graphite used in the composite. Data on dynamic elastic modulus, thermal expansion, thermal conductivity, and thermal-stress fracture resistance are presented.

I. INTRODUCTION

A continuing interest in carbide-graphite composites prevails at the Los Alamos Scientific Laboratory (LASL) of the University of California due to the useful characteristics of these materials under extreme temperature conditions. The tantalum carbide-graphite system has evoked particular interest due to the extremely high melting point of TaC (3900°C) and the high TaC-C eutectic temperature of 3710°C. Previous work [1-4] by the LASL Materials Technology Group (CMB-6) has provided insight into the effect of processing variables, carbide powder characteristics, composition, binder content, and graphite particle characteristics upon the physical and mechanical properties of hot-pressed carbide-graphite composites in general, and upon TaC-C composites in particular.

The purpose of this investigation was to develop an alternative process to hot pressing for the production of TaC-C composite material, and to determine and compare selected properties of materials prepared in each manner. A procedure for hydrostatically pressing and subsequently heat treating compacts of TaC and graphite was developed, and various techniques were utilized to evaluate the materials produced in this manner and by hot pressing. Also, three different size ranges of graphite were hydrostatically pressed and tested for future reference and possible applicability to carbide-graphite systems. The evaluations of physical structure and thermal properties, particularly thermal-shock capabilities, were of most interest during this in investigation. Particular attention was paid to the effect of carbide content and carbide particle size.

II. MATERIALS

The raw materials used in the investigation comprised several lots of TaC, one of NbC, three size ranges of graphite, and Varcum binder.

A. Tantalum Carbide (TaC) Powders

Analyses and characteristics of the TaC powders used are presented in Tables I and II, respectively. Five of the powders used are shown in the photomicrographs of Figs. 1 through 5. Scanning electron micrographs of the nominal 300-Å TaC (TaC-38) powder are shown in Figs. 6 through 8.

B. Niobium Carbide (NbC) Powder

The NbC powder, Lot NbC-43, was purchased from Wah Chang Chemical Company. This powder lot had a Fisher average particle size (APS) of 3.51 μm, a bulk density of 2.61 g/cm^3, a tap density of 3.82 g/cm^3, and specific surface area measurements of 0.219 and 1.205 m^2/g for Fisher and BET determinations, respectively. Chemical analysis revealed 88.4% niobium, 11.3% total carbon, 0.33% free carbon,

TABLE I

CHEMICAL ANALYSES OF TaC POWDER LOTS[a]

Elements	TaC-11	TaC-15	TaC-29	TaC-30	TaC-32	TaC-33	TaC-38	TaC-45
Ta	93.3%	92.9%	93.44%	93.81%	93.34%	92.0%	90.8%	93.6%
Total C	6.25%	6.70%	5.98%	6.10%	6.30%	6.30%	7.30%	6.20%
Free C	0.08%	0.65%	< 500	790	780	0.50%	1.70%	0.10%
O_2	0.21%	570	0.19%	0.18%	0.17%	1.40%	1.70%	580
Li	< 1	< 3	< 1	< 3	< 1	< 3	< 1	< 1
Be	< 1	< 1	< 1	< 1	< 1	< 1	< 1	< 1
B	3	< 3	< 3	< 3	< 3	< 3	< 3	< 3
Na	< 3	< 3	< 3	< 3	< 3	< 3	< 3	< 3
Mg	3	1	15	15	< 1	2	20	< 1
Al	< 3	< 3	5	3	10	< 3	15	10
Si	100	5	10	5	5	10	15	10
K	< 10	< 30	< 10	< 10	< 10	< 30	< 10	< 10
Ca	3	3	3	2	5	3	2	3
Ti	< 5	< 5	< 5	< 5	150	10	10	50
V	< 10	< 10	< 10	< 10	< 10	10	< 10	< 10
Cr	5	5	10	10	0.1%	300	600	300
Mn	1	< 1	2	< 1	2	10	10	3
Fe	200	50	150	150	50	300	800	500
Co	< 5	< 5	< 5	< 5	200	< 5	< 5	200
Ni	1	20	< 5	2	30	100	0.1%	300
Cu	30	< 1	2	2	8	15	10	< 1
Zn	< 100	< 100	< 100	< 100	< 100	< 100	< 100	< 100
Sr	< 30	< 30	< 30	< 30	< 30	< 30	< 30	< 30
Y	< 30	< 30	< 30	< 30	< 30	< 30	< 30	< 30
Zr	< 30	< 30	< 30	< 30	< 30	< 30	< 30	< 30
Nb	0.1%	0.3%	500	200	0.2%	200	0.75%	300
Mo	< 10	< 10	< 10	< 10	50	10	< 10	< 100
Ag	< 1	< 1	3	< 1	< 1	< 1	< 1	< 1
Sn	< 3	< 3	< 3	< 3	< 3	< 3	< 3	< 3
Ba	< 10	< 10	< 10	< 10	< 10	< 10	< 10	< 10
W	< 30	< 30	< 30	< 30	0.3%	200	50	< 30
Pb	< 3	< 3	< 3	10	< 3	< 3	< 3	< 3
Bi	< 5	< 5	< 5	< 5	< 5	< 5	< 5	< 5

[a]All values are ppm unless otherwise indicated.

TABLE II

TaC CHARACTERIZATION DATA

Powder Lot	Supplier	Density Bulk (g/cm^3)	Density Tap (g/cm^3)	Fisher APS (μm)	Specific Surface BET (m^2/g)	Specific Surface Fisher (m^2/g)
TaC-11	Rembar	6.04	8.01	4.2	0.616	0.098
TaC-15	Union Carbide	1.90	3.20	0.13	3.22	
TaC-29	Kawecki	4.59	6.31	1.30	1.305	0.315
TaC-30	Kawecki	4.51	6.42	1.37	1.109	0.299
TaC-32	Starck	5.13	8.00	1.85	0.712	0.410
TaC-33	Ciba	--	--	300 Å	17.524	--
TaC-38	Starck	--	--	300 Å	41.614	--
TaC-45	Starck	5.14	6.61	8.6	0.498	0.048

and 0.31% oxygen. This material was used in 50/50 wt% solid solution with TaC, and was included for comparison purposes.

C. Graphite Flours

1. M-3 Graphite Flour. The graphite flour used in this program was Grade 1008, supplied by Great Lakes Carbon Company, and was given the LASL identifying number M-3. Typical chemical analyses and size distribution of the as-received flour are presented in Tables III and IV, respectively. The bulk of the graphite used in this examination was the -325 fraction of the M-3 flour, which was the portion used in the carbide-graphite composite material and as one of the size ranges used for investigation of pure graphite materials. Pure graphite specimens used were the -150 +325 mesh fraction and a standard mix composed of 85% (by weight) M-3 flour and 15% Thermax.

2. S-97 Graphite Flour. The second graphite used, obtained from Speer Carbon Company, was designated S-97. The chemical analyses of this flour and the particle size distribution are given in Tables III and IV, respectively.

D. Thermax

Thermax is a carbon black of 0.9-μm average particle size obtained from Thermatomic Carbon Co..

TABLE III

CHEMICAL ANALYSES OF GRAPHITE FLOURS

Impurity[a]	M-3 Flour (ppm)	S-97 Flour (ppm)
Ash	300	100
Iron	100	70
Silicon	150	30

[a]All others less than 200 ppm total.

TABLE IV

PARTICLE SIZE DISTRIBUTION OF GRAPHITE FLOURS

Mesh Size	M-3 Flour (Wt%)	S-97 Flour (Wt%)
+65	3	0
-65 +100	5	0
-100 +150	11	0
-150 +200	26	0
-200 +270	10	10
-270 +325	15	20
-325	30	70

The chemical analyses of this material are shown in Table V.

E. Varcum Binder

When a binder was needed, we used Varcum 8251, a thermosetting resin of partially polymerized furfuryl alcohol obtained from the Varcum Chemical Division of Reichhold Chemicals, Inc. Maleic anhydride was used as a catalyst in the amount of 4 g per 100 cm^3 of resin. The viscosity of this material at room temperature is about 300 cP, and decreases rapidly to about 50 cP at 50°C.

III. EQUIPMENT

A. Blenders

A Patterson-Kelly 8- or 16-qt twin shell blender equipped with an intensifier bar and liquid addition apparatus was used for dry ingredient mixing and liquid binder addition. The 16-qt blender is shown in Fig. 9. For the hot-pressing blends with

TABLE V

CHEMICAL ANALYSES OF THERMAX

Impurity[a]	Amount (ppm)
Ash	700 - 2000
Si	100 - 620
Fe	30 - 50
Ca	10
Mg	5 - 10
Na	5 - 10
Al	3 - 10
Mn	1 - 5

[a]All other elements below detection limits of spectrochemical analysis.

no binder, mixing was done in glass jars containing aluminum agitator wires.

B. Homogenizer

A Hobart Model 4532 meat chopper equipped with a breaker plate with 1/8-in.-diam holes was used for homogenizing and precompacting the hydrostatic pressing mixes (Fig. 10).

C. Pressings Sacks

The pressing sacks and lids were furnished by the LASL Plastics Section of Group CMB-6 and were made of Plastisol. These sacks were formed by dipping a mandrel into Plastisol and curing at 175°C for 45 min.

D. Hydrostatic Press

The loaded pressing sacks were pressed by hydrostatic pressure of 30,000 psi in a 12-in.-i.d. by 24-in.-long chamber utilizing oil pressurized by an air operated pump (Fig. 11).

E. Curing Oven

The hydrostatically pressed pieces were cured in an oven capable of maintaining the rigid time-temperature schedule outlined in Section IV. F. The unit used was an electrically heated circulating air oven capable of sustained operation at up to 450°C. The oven, Model FO 962430, was made by the Cooley Electrical Manufacturing Company, and was controlled by a cam-operated Wheelco Instrument Company controller. The oven, along with the containers that held the pressings, is shown in Fig. 12.

F. Baking Furnace

The cured pieces were baked under vacuum to 800°C as indicated in Section IV. G. The pieces were placed inside a stainless steel can and were baked in a furnace designed and built at LASL. The furnace was heated by resistance heating elements controlled by a cam-operated Wheelco controller. The hot zone of the furnace was 16 in. diam by 60 in. long; the furnace normally operated under a pressure of 10 torr or less. The vacuum system consisted of a two-stage Nash Hytor pump: two Model TS-10 pumps connected in series, but powered by a single 10-hp electric motor. An air-operated valve in the vacuum line prevented air from being drawn into the furnace through the vacuum pump in case of a power failure. Also, a self-opening trap prevented the vacuum pump water from entering the furnace. The baking furnace is shown in Fig. 13.

G. Sintering Furnace

Following baking, the pieces not to be hot pressed were heat treated to 2500°C according to the schedule described in Section IV. H. They were placed in a graphite crucible and sintered in an induction heated furnace designed and built at LASL. The induction coil was powered by a 175-kW 960-cycle motor generator set. The 82-in.-long coil consisted of flat 6-in.-wide copper strips bent and silver-soldered together to form a cylinder. Three parallel copper tubes to carry cooling water were silver-soldered to the outside of the coil. The crucible containing the pressings was located within a graphite susceptor, 18.75-in.-o.d. by 16.62-in.-i.d. The susceptor, in turn, was surrounded by a 3-in.-thick layer of carbon black insulation, a 1-in.-thick ceramic liner, a layer of Fiberfrax, and the induction coil. The temperature in the furnace was measured optically through a sight port in the top of the furnace that sighted into a hole in the graphite crucible. A helium flush kept the sight port open and prevented the graphite in the furnace from oxidizing. The induction furnace is shown in Fig. 14.

H. High-Temperature Sintering Furnace

Following sintering, some of the pieces were subjected to a higher temperature heat treatment similar to that described in Section IV. I. The furnace used for this purpose was capable of operating at 3000°C for a sustained period. The pieces produced at LASL were heat treated in graphite crucibles in an induction furnace (Fig. 15) designed and built at LASL. The coil was a self-shielded, light-tight, current-concentrating coil powered by a 150-kW 10,000-cycle motor generator set. Temperature was measured by sighting through a hole in the crucible lid directly on the piece. An argon flush kept the sight port open and prevented oxidation.

I. Hot-Press Furnaces

The hot-press furnaces used (Fig. 16) were of the induction heated type shown in Fig. 17.

IV. PROCEDURE

A. Preparation of Materials

Before use, the graphite and carbide powders were screened through a 150-mesh screen to ensure against introduction of foreign particles. Also, they were dried for 24 h at 150°C to minimize

the presence of water vapor and to help prevent agglomeration. The binder resin was stored in 55-gal drums. The drums to be used were then rolled in the storage area at 400 rpm for 2 h to homogenize the material before withdrawal. The quantity of resin required for a day's work was withdrawn from the drum the evening before use and was placed overnight in an oven at 35°C. The maleic anhydride catalyst was ground and screened to -20 mesh prior to use, and 4 g of catalyst per 100 cm^3 of resin was added to the original resin. The mixing was performed in 1-gal batches; the mix was heated to 40°C and stirred for approximately 20 min before use. Maleic anhydride is a slow-acting catalyst at 40°C so the processing times were not critical.

B. Blending

The dry ingredients (graphite, or graphite and TaC) for the 8-qt Paterson-Kelly blender were in the range of 1 to 4 kg to ensure good blending. The dry ingredients for a mix were weighed and placed in the blender: the TaC first and the graphite last. They were dry blended for 30 min using the intensifier bar. The proper amount of catalyzed resin was weighed and placed in a glass reservoir wound with a heating tape. The reservoir had a tube leading to the liquid addition apparatus of the Patterson-Kelly blender. The resin, after heating to approximately 40°C, was added slowly under 3-psi air pressure to the dry mix over a period of 15 to 20 min through the intensifier bar of the blender. After the resin addition was completed, the blender was stopped, the lids opened, and the lids and blender walls were scraped to remove adhering material. The blender was then sealed and rotated for another 5 min with the intensifier bar operating. The blended material had the consistency of moist sand.

C. Homogenization

The blends containing no binder went directly to the screening step, but the ones containing Varcum underwent the following homogenization, probably the most important single step for ensuring the homogeneity and distribution desired in the final product. A Hobart meat chopper was used to homogenize the mix, which was passed through the meat chopper six times before being loaded into the pressing sacks. Normally the meat chopper is fitted with a chopper plate having 3/16-in.-diam holes. A plate with 1/8-in.-diam holes, however, was used for these mixes to improve the mixing and homogenization obtained.

D. Screening

Following the homogenization operation, the mix was forced through a 20-mesh screen to break up large clusters and to give the mix better flow properties for loading into the pressing sacks.

E. Hydrostatic Pressing

The parts comprising a pressing sack (Fig. 18) included the sack and lid, clamping ring, Aero Seal clamp, hypodermic needle, sponge, and mix. The pressing sacks were filled with the loose screened mix, and the mix was packed lightly by tapping the filled sacks. More loose material was then added, and the procedure was repeated several times until no compaction was noted. The sack lid was pierced with a No. 16 hypodermic needle with a 7/8-in.-diam by 1/2-in.-thick sponge affixed to the needle point. A clamping ring was then placed around the inner diameter of the lid and the lid seated in the sack. The sack was sealed with an Aero Seal hose clamp and a sealing solution described below. The sack and its contents were then evacuated through the protruding hypodermic needle, usually for 1/2 h (Fig. 19). The needle was extracted from the lid and the hole sealed with a solution of poly-vinyl-chloride in equal parts of methyl, ethyl, ketone, and acetone. The loaded and evacuated sacks were then placed in the pressure chamber, oil added, and the chamber closed. The air-operated oil pump was started, and the chamber was pressurized to the required pressure. The pressure was immediately released and the chamber opened. Oil was removed from the exterior of the sacks with hexane before they were opened.

F. Curing

The green pressings were cured according to the time-temperature schedule shown in Table VI. Curing resulted in the polymerization of the thermosetting binder. This process occurred in an air atmosphere; the pieces were merely wrapped in aluminum foil and placed inside the oven. The 1°C/h rate was very important in the range where volatiles from polymerization were being released.

G. Baking

The cured pressings were then baked under vacuum according to the schedule given in Table VI to carbonize the binder and further remove gases and volatiles. Baking was done inside a stainless steel can with a loose-fitting lid.

TABLE VI

TIME AND TEMPERATURE SCHEDULES FOR CURING AND BAKING

Time (h)	Cure Temp (°C)	Cure Rate (°C)	Bake Temp (°C)	Bake Rate (°C)
3	53	1	250	10
6	56	1	280	10
9	59	1	310	10
12	62	1	340	10
15	65	1	370	10
18	68	1	400	10
21	71	1	430	10
24	74	1	460	10
27	77	1	490	10
30	80	1	520	10
33	83	1	550	10
36	86	1	580	10
39	89	1	610	10
42	92	1	685	25
45	95	1	760	25
48	98	1	835	25
51	101	1		
54	104	1		
57	107	1		
60	110	1		
62	112	1		
65	118	2		
68	124	2		
71	130	2		
74	142	4		
77	160	6		
80	180	6-2/3		
83	200	6-2/3		
86	225	8-1/3		
89	250	8-1/3		

Following this step the pieces to be hot pressed were advanced to the hot-pressing step described in Section IV. J.

H. Sintering

A sintering run to 2500°C followed the baking cycle. The baked pressings were placed in a graphite crucible that, in turn, was placed in the induction heated sintering furnace. The pressings were heated to 2500°C over 4-1/2 h and held at temperature for 2 h. A helium atmosphere was maintained in the furnace during this period and during the 1-1/2-day cooling cycle. Heat treatment of the pure graphite pieces ended here. All pieces undergoing sintering were machined to right cylinders following this step.

I. High-Temperature Heat Treatment

Following the sintering cycle, the pressings containing TaC and graphite were heat treated at 3000°C for 1 h. The pieces were heated rapidly to 3000°C using a 40-min ramp. An argon atmosphere protected the pieces from oxidation.

J. Hot Pressing

The hot-pressed pieces underwent this process following the baking step. The hot-pressing schedule employed was as follows: after the die was loaded, positioned in the induction coil, and flushed with argon, it was heated to 3050°C in 40 min while a pressure of 3200 psi was gradually applied. Pressure was maintained for about 30 to 40 min, following which the power was shut off and the die allowed to cool. Pressure was not released until the temperature fell below 2000°C.

V. COMPOSITIONS

A. TaC-Graphite

The various compositions investigated are given in Table VII. A 50% coking value was used in batch calculations to indicate the Varcum contribution to the carbon content. Varcum demands varied depending on the percentage of carbide in the mix and the particle size of the carbide used. The requirements ranged from 20 to 23% of the dry ingredient weight. Binder demands might vary considerably from this figure if the particle size of the graphite used were to be changed.

TABLE VII

TaC GRAPHITE COMPOSITIONS

Nominal TaC APS (μm)	1 Wt%	5 Wt%	7 Wt%	14 Wt%	20 Wt%	40 Wt%
40.0	S	S	S	S	S	S
4.2						H
1.3	S	S	S	S		S, H
0.13						H
300 Å	S	S	S	S	S	H

S - hydrostatically pressed and sintered; H_2-hot pressed.

TABLE VIII

SAMPLE DESCRIPTIONS

Sample No.	Wt% Carbide	TaC Particle Size	Graphite Size[a] and Source	Fabrication[b] Technique	Density (g/cm^3)	% Theo Density
2111A	40	0.13 μm	-325 M-3	Hot Pressed	2.65	78.0
2108A	40	4.2 μm	-325 M-3	Hot Pressed	2.66	78.3
2106A	40	300 Å	-325 M-3	Hot Pressed	2.65	78.0
2141A	40	1.3 μm	-325 M-3	Hot Pressed	2.74	80.6
S-4006D[c]	10 vol%	NbC 3.5 μm, TaC 1.65 μm	-150 +325 M-3	Hot Pressed	2.71	82.9
101	40	300 Å	-325 M-3	Sintered	2.54	74.7
102	40	1.3 μm	-325 M-3	Sintered	2.47	72.7
0924	None	None	-200 mesh S-97	Sintered	1.825	81.1
E-001	None	None	85 wt% M-3, 15 wt% Thermax	Extruded and Sintered	1.875	83.3
0941-4	None	None	-325 M-3 + Varcum	Sintered	1.46	64.9
0941-16	None	None	85 wt% -325 M-3, 15 wt% Thermax	Sintered	1.76	78.3
0941-19	None	None	-150 +325 M-3	Sintered	1.43	63.6
0938-1	1	300 Å	-325 M-3	Sintered	1.52	67.0
0938-5	5	300 Å	-325 M-3	Sintered	1.60	68.1
0938-7	7	300 Å	-325 M-3	Sintered	1.63	68.2
0938-14	14	300 Å	-325 M-3	Sintered	1.78	69.7
0938-20	20	300 Å	-325 M-3	Sintered	1.91	70.6
0939-1	1	1.3 μm	-325 M-3	Sintered	1.55	68.3
0939-5	5	1.3 μm	-325 M-3	Sintered	1.60	68.1
0939-7	7	1.3 μm	-325 M-3	Sintered	1.80[d]	75.3
0939-14	14	1.3 μm	-325 M-3	Sintered	1.75	68.6
0939-40	40	1.3 μm	-325 M-3	Sintered	2.52	74.2
0940-1	1	40.0 μm	-325 M-3	Sintered	1.52	67.0
0940-5	5	40.0 μm	-325 M-3	Sintered	1.57	66.8
0940-7	7	40.0 μm	-325 M-3	Sintered	1.60	66.9
0940-14	14	40.0 μm	-325 M-3	Sintered	1.75	68.6
0940-20	20	40.0 μm	-325 M-3	Sintered	1.86	68.7
0940-40	40	40.0 μm	-325 M-3	Sintered	2.40	70.6

[a] -325 M-3 has an average particle size of ~4.2 μm. -150 +325 M-3 has an average particle size of ~70 μm.

[b] Sintered pieces, except where noted, were formed by hydrostatically pressing.

[c] 39.7 wt% TaC-39.7 wt% NbC-20.6 wt% C solid-solution composite.

[d] Unusually high, unexplained.

B. Graphite

The various graphites investigated are as follows: -200 mesh S-97, -325 mesh M-3, standard mix (85 wt% M-3 + 15 wt% Thermax), and -150 +325 mesh M-3. A sample of extruded standard mix that was cured, baked, and graphitized was also included for comparison.

Descriptions of all samples tested are presented in Table VIII, and both graphite and TaC-C samples are included.

VI. TESTING

The thermal-stress and thermal-shock capabilities of materials in this investigation were determined by using two methods that established temperature gradients in material samples and established

power or temperature levels necessary to initiate cracking or fracture. The first method, thermal-stress method,[5] was a steady-state test utilizing a flat washer specimen, 1.2-in.-o.d. by 0.5-in.-i.d. by 1/16-in.-thick, supported on its inside diameter by a water-cooled copper probe thermally coupled to a heat sink by copper conduction washers (Figs. 20 and 21). The outer rim of the washer received a heat flux by thermal radiation from a graphite radiator and the radial temperature gradient was created in the sample. Slow heating precluded any significant temperature transients. Successive radiator temperatures were tried (using different samples for each) until that temperature was achieved where a radial crack was initiated at the inside diameter of the sample. The crack initiation temperature (CIT) was the value reported.

The thermal-shock test induced heat in the outer rim of a washer, 1.0-in.-o.d. by 0.25-in.-i.d. by 1/16-in.-thick, by means of an rf induction heating apparatus. The outer rim heated rapidly, producing a gradient between the inside and outside diameters, which equilibrated in about 1 sec. The rapid and large initial temperature difference produced the thermal shock. The failure manifested as a crack during the power application. The thermal-shock index (TSI) reported was simply the power setting of the rf power supply.

Both steady-state and thermal-shock data were taken on washer samples whose planes were in the "with-grain" direction (perpendicular to the direction of pressing) for hot-pressed material. Hydrostatically pressed materials were isotropic.

The coefficient of thermal expansion and dynamic-modulus measurements were made in an elastic-modulus furnace constructed from a design by H. L. Brown and P. E. Armstrong of LASL Group CMF-13. This furnace was used simultaneously to measure elastic modulus and CTE of samples to temperatures of 2500°C. The modulus-CTE furnace shell was a 6-3/4 in. inside diameter, 11-1/4 in. inside length, horizontal water-cooled cylinder slit lengthwise. The sample, 1/4-in.-diam by 4-in.-long, with axis parallel to the pressing direction (where applicable) was supported in the center of a cylindrical radiator by three pointed graphite screws attached to a graphite ring which in turn was fastened at the center of the lower half of the radiator. When the furnace was closed, the radiator and the shields surrounding it formed a cylindrical cavity around the specimen with a small horizontal slit through which the sample could be observed. The cross section of the radiator was varied to provide thinner sections on its ends. The hotter ends of the radiator thus achieved just offset the sample heat loss to the partially open ends of the radiator cylinder. Tests were conducted in an argon atmosphere at a pressure of about 2 in. of water.

Power was provided by a 45-KVA Burton Power Supply operating on single phase 60 cycle AC current. Temperature was measured up to about 1200°C by a Chromel-Alumel thermocouple contacting the sample support ring. Above 1200°C, temperature inside the furnace was measured with a Leeds & Northrup optical pyrometer sighting on the sample surface through the center part of the furnace.

The change in length of the specimen was measured using twin microscopes to view two fiducial marks on the specimen. The modulus was measured by passing an ultrasonic sound wave through the sample and measuring the vibrations.

Both phenomenas were measured simultaneously in the following manner. The sample was heated to a desired temperature, the temperature was stabilized, and the driver and pickup wires were coupled into holes in the sample. Using a micrometer drive, the wires were adjusted to yield maximum signal transfer to and from the sample. Next, the spectrum was scanned for proper reasonance frequency and the overall length of the specimen was measured with the twin microscopes. The modulus is proportional to the square of the reasonance frequency and may be calculated. At each stabilized temperature the change in the specimen length was measured to determine thermal expansion characteristics.

Thermal-conductivity measurements were made using a probe comparator apparatus comprising a tungsten hemisphere and adjacent thermocouple. Measurements were made on experimental material and calibrated against a known standard. The samples were 1 in. diam by 1/4 in. thick.

VII. DISCUSSION OF RESULTS

The first group of samples tested was made up of hot-pressed material containing 40 wt% (10 vol%) TaC of differing particle sizes, or, in the case of

Sample S-4006D, 10 vol% of a 50/50 wt% solid solution of NbC-TaC. This NbC-TaC sample was included for comparison. The samples tested (2111A, 2108A, 2106A, 2141A, and S-4006D) are described, as are all tested samples, in Table VIII. This description includes composition, TaC size if applicable, fabrication technique, and densities. Preliminary investigation of structure by conventional metallographic means indicated excellent distribution of TaC particles within the graphite phase (Fig. 22). This was confirmed by subsequent scanning electron micrographs presented in Figs. 23 through 28. The desired chemical analyses and actual chemical analyses of some samples of this group are presented in Table IX. Good composition control was achieved.

TABLE IX

TYPICAL ANALYTIC RESULTS ON SELECTIVE SAMPLES OF THE 40 WT%(10 VOL%) TaC-CARBON COMPOSITES

Sample No.	Desired Analyses Ta (%)	Desired Analyses Total C (%)	Desired Analyses Free C (%)	Actual Analyses Ta (%)	Actual Analyses Total C (%)	Actual Analyses Free C (%)
2106 A	37.5	62.5	60.0	37.0	42.9	61.7
2108 A	37.5	62.5	60.0	37.9	61.7	59.3
2111 A	37.5	62.5	60.0	37.5	62.4	59.8

Testing results of thermal properties are presented in Table X. Values for all samples tested are present. Values are omitted only if sample material was not available. From the hot-pressed composite, samples listed above, several conclusions were drawn. It appeared that 2111A (0.13 μm), 2141A (1.3 μm), and 2108A (4.2 μm) were similar in thermal-fracture resistance, and that 2106A (300 Å) had much poorer resistance. Thermal-stress resistance seems to increase with increasing carbide particle size although it is less pronounced with the three larger-sized particles than with the 300-Å material. All TaC-C composites were significantly less resistant than the solid-solution composite (S-4006D), probably due to the Varcum binder in the TaC samples and other differences in the graphite phase.

Determinations of dynamic elastic (Young's) modulus and thermal expansion results are presented in Table X, whereas Figs. 29 through 33 show some of the temperature dependences of these properties. Modulus behavior for the TaC-C composites was quite similar to the NbC-TaC-C material, but the thermal expansion values were much lower.

Materials of the same composition were then produced utilizing hydrostatic pressing and sintering rather than hot pressing (Samples 101 and 102). The results showed little change in thermal-fracture resistance from the hot-pressed materials. The only change discernable was a slight improvement in the samples tested under steady-state conditions. Lower densities than those found in the hot-pressed materials were noted.

Testing hydrostatically pressed and sintered graphites produced an interesting trend. In the previously tested materials containing TaC, an increase in thermal-shock index was accompanied by a concomitant increase in crack initiation temperature, but this was not true for the graphites tested. In fact, the graphite with the highest TSI (-200 mesh S-97) had the lowest CIT; and conversely, the graphite with the highest CIT (-150 +325 mesh M-3) had the lowest TSI. Although marked differences in structure can be seen in the photomicrographs and scanning micrographs of Figs. 34 through 39, little difference exists in TSI except with the S-97. CIT values, however, indicate better performance by the -150 +325 mesh M-3. Unfortunately no photomicrograph of the -200 mesh S-97 structure is available for comparison. The high room-temperature modulus of the S-97 sample was compared with that of an extruded standard mix to check for comparable values, and was found to be lower.

In the final phase of this investigation, samples were made varying both the particle size and the amount of TaC used in the composite material. Carbides of 300 Å, 1.3 μm, and 40 μm nominal particle sizes were used in amounts ranging from 1 to 40 wt%. Conventional and scanning electron micrographs are presented of the composite material containing 300-Å, 1.3-μm, and 40-μm TaC in Figs. 40 through 49, Figs. 50 through 59, and Figs. 60 through 71, respectively. They reveal the excellent distribution of carbide in the graphite. The thermal-shock test showed that the coarse TaC produced the best thermal-fracture resistance. Indeed, by using particles differing in size by at least an order of magnitude, a distinction could easily be made between the thermal-stress resistance improvement of each size range.

A tangential study demonstrated the need for thermally shocking a specimen only once. It asserted that when specimens are shocked more than once, they can withstand greater thermal shocks than virgin ma-

TABLE X

EXPERIMENTALLY DETERMINED PROPERTIES OF TaC-C COMPOSITES AND GRAPHITES[b]

Sample No.	Thermal Shock Index (TSI)[a]	Crack Initiation Temp (CIT)	Room Temp Elastic Modulus (AG) $lb/in^2 \times 10^6$	Mean Coefficient of Thermal Expansion (20-2000°C)(AG) $\times 10^{-6}/°C$	Thermal Conductivity (at 33°C) W/m-K
2111 A	415/435	2000	1.131	6.638	--
2108 A	430/435	2055	1.054	6.357	--
2106 A	390/395	1840	--	--	--
2141 A	420/425	1985	1.174	6.645	--
S-4006D	460/465	2370	1.167	7.792	--
101	395/400	1885	--	--	--
102	420/425	2050	--	--	--
0924	400/405	1405	1.526	4.783	--
E-001	--	--	2.339	3.670	--
0941-4	305/307.5	1740	--	--	1.40
0941-16	310/312.5	1860	--	--	1.28
0941-19	300/302.5	1920	--	--	1.28
0938-1	--	< 1475	--	--	--
0938-5	--	1700	--	--	1.44
0938-7	--	1950	--	--	--
0938-14	312.5/315	--	--	--	--
0938-20	297.5/300	1825	--	--	--
0939-1	280/282.5	1890	--	--	1.35
0939-5	300/305	1680	--	--	1.43
0939-7	297.5/315	1990	--	--	1.39
0939-14	335/337.5	1970	--	--	--
0939-40	320/322.5	1910	--	--	1.39
0940-1	300/302.5	< 1570	--	--	1.40
0940-5	335/337.5	1885	--	--	1.40
0940-7	347.5/350	--	--	--	--
0940-14	345/350	2100	--	--	1.39
0940-20	325/327.5	1955	--	--	1.41
0940-40	337.5/340	2000	--	--	1.33

[a]The first number indicates the highest power setting prior to one that initiated cracking. The second number indicates the power setting at which cracking occurred. Because a number of samples are run, more than one increment may separate the two numbers.

[b]Omitted values indicated no sample available for testing.

terial. Table XI shows the effect of repeatedly subjecting specimens to increasingly higher levels of thermal shock. Recycled specimens fracture at higher power levels than do virgin materials.

Probably the most meaningful information generated in the final phase investigation came from

TABLE XI

THERMAL SHOCK RECYCLING

Sample No.	TSI	Cycling Runs-Power Settings Run 1	Run 2	Run 3	Run 4
0940-14	345/350	320	340	360	380[a]
0940-20	325/327.5	320	340	360[a]	
0940-40	337.5/340	320	340	360	380[a]

[a]Fracture.

TABLE XII

THERMAL STRESS FRACTURE RESISTANCE

Sample No.	CIT (°C)	ϵ_s	λ_s (W/cm°K)[a]	TGI x 10^{-12}	Rating[b]
0941-4	1740	0.70	1.40	8.2	1.0
0941-16	1860	0.70	1.28	11.0	1.3
0941-19	1920	0.70	1.28	13.0	1.6
0938-1	< 1475	0.90	(1.44)[c]	6.0	< 0.73
0938-5	1700	0.90	1.44	9.0	1.1
0938-7	1950	0.90	(1.44)	15.0	1.8
0938-20	1825	0.90	(1.44)	12.0	1.5
0939-1	1890	0.90	1.35	15.0	1.8
0939-5	1680	0.90	1.43	9.0	1.1
0939-7	1950	0.90	1.39	17.0	2.1
0930-14	1970	0.90	(1.39)	16.0	2.0
0939-40	1910	0.90	1.39	15.0	1.8
0940-1	< 1570	0.90	1.40	7.0	< 0.85
0940-5	1885	0.90	1.40	14.0	1.7
0940-14	2100	0.90	1.39	21.0	2.6
0940-20	1955	0.90	1.41	16.0	2.0
0940-40	2000	0.90	1.33	18.0	2.2

[a] Room temperature values.

[b] Relative to basic graphite matrix, 0941-4.

[c] Assumed.

the steady-state thermal-stress fracture studies and the thermal-conductivity measurements. Previous steady-state tests produced a crack initiation temperature used to rank materials. These CIT's did not give quantitative comparisons of thermal-fracture resistances, but instead gave only rankings. A new thermal-stress fracture resistance was introduced in this final phase. This parameter, TGI,[6] depends upon the emissivity, thermal conductivity, and CIT, and is a function of the relative temperature gradient existing in the sample at crack initiation. This parameter may be used in a quantitative sense to rate materials and to ascertain how much better one is than another. The expression for this parameter is as follows.

$$TGI = \frac{\epsilon_s (CIT)^4}{\lambda_s}$$

where ϵ_s = emissivity,

CIT = crack initiation temperature, and

λ_s = thermal conductivity.

The values of TGI are presented in Table XII. In addition to the TaC-C composites of this phase of the investigation, the TGI's for the graphites of the previous phase are offered. The final column of Table XII is a rating relative to the basic -325 mesh M-3 graphite matrix that was present as 0941-4.

Adding TaC improved the thermal-stress fracture resistance of the composite material in all but two cases. In addition, the larger the size of the TaC particle, the higher the thermal-stress fracture resistance; the highest resistance being 40-μm TaC particles. No explanation is available for the extremely low thermal-stress fracture resistance of materials 0938-1 and 0940-1. The highest fracture resistance of any material tested was for the specimen containing 14 wt% of 40-μm TaC. For each particle size range, the maximum thermal-stress fracture resistance occurred at intermediate levels of TaC addition, either 7 or 14 wt%. For the pure graphite samples, the -150 +325 mesh M-3 appeared to be the most resistant to thermal-stress fracture.

VIII. CONCLUSIONS

From this study it became evident that TaC-C composites or 100% graphite materials could be produced in a well-controlled manner, the materials exhibiting little variability with respect to density, carbide particle distribution, chemistry, modulus, thermal expansion, and thermal shock characteristics in samples of similar composition.

Thermal properties were investigated both to establish baseline values and to understand the effects of variables upon these values. It became evident that the particle size of the carbide affected the thermal-expansion characteristics of the material and the elastic modulus and that thermal-stress fracture resistance was dependent upon the size and relative amounts of both the TaC and graphite in the composite.

Thermal expansion of samples differing only in the particle size of carbide used was greater for the specimens containing the finer TaC, but was much lower than the NbC-TaC solid solution graphite composite tested. Dynamic elastic modulus of the specimens containing the finer TaC was higher than its coarse counterpart, and both showed a close relationship to the NbC-TaC-C material. Adding TaC to graphite appears to improve the thermal-stress fracture resistance of the graphite, the larger the size of the TaC particle the greater the fracture resistance induced. Of the pure graphites tested, the -150 +325 mesh fraction appeared to be the most resistant to thermal-stress fracture.

ACKNOWLEDGMENTS

The authors express appreciation to the following LASL people for their assistance in this investigation: T. I. Jones and C. Javorsky of the Physical Metallurgy Section for conventional metallography; S. Sandoval for illustrations; R. Andrae, C. King, C. Saunders, and W. Sibbitt of Group M-7 for thermal-stress fracture, thermal expansion, and thermal conductivity measurements; Group CMB-1 for chemical analyses; J. Magnuson for powder characterization; T. Gregory for scanning electron microscopy; A. Lovato for hot pressing; the Shops Department for machining of samples; and H. Sheinberg and J. T. Frakes for supervision of the billet manufacture.

REFERENCES

1. K. V. Davidson, R. E. Riley, and J. M. Taub, "Carbide-Graphite Composites," Los Alamos Scientific Laboratory report LA-3569-MS (Oct. 1966).
2. K. V. Davidson, R. E. Riley, and J. M. Taub, "The Effect of Contaminants on the High Temperature Properties of Carbide-Graphite Composites," Los Alamos Scientific Laboratory report LA-3618-MS (Jan. 1967).
3. K. V. Davidson, R. E. Riley, and J. M. Taub, "Carbide-Graphite Composites. Second Progress Report," Los Alamos Scientific Laboratory report LA-3652-MS (June 1967).
4. R. E. Riley, N. K. Richerson, and D. H. Schell, "Extruded Carbide-Graphite Composites," Los Alamos Scientific Laboratory report LA-4077 (Feb. 1969).
5. A. E. Carden and R. W. Andrae, "Thermal-Stress Crack Initiation Method of Ranking Ceramic Materials," J. Amer. Ceramic Soc. 53, No. 6 (June 1970).
6. R. W. Andrae, Los Alamos Scientific Laboratory internal document (April 1971).

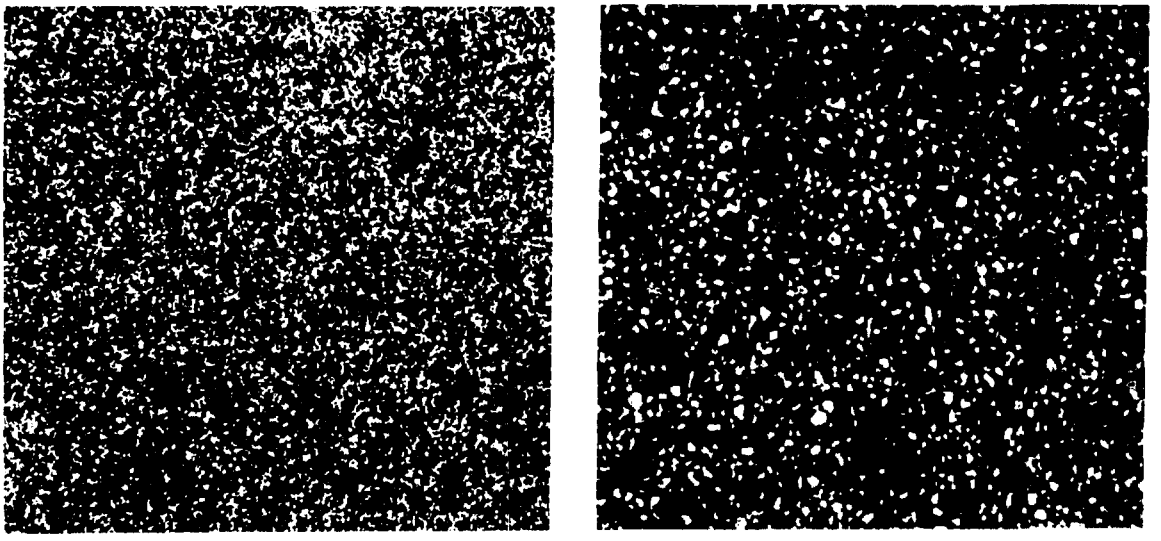

Fig. 1. Powder TaC-11, nominal 4.2-μm average particle size. (Conventional metallography. Left, 100X. Right, 250X.)

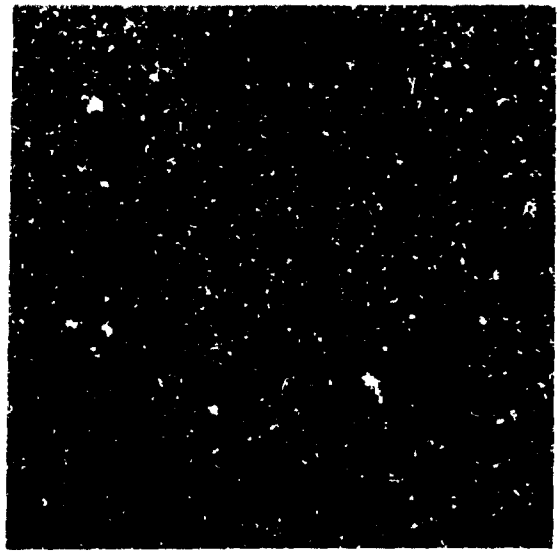

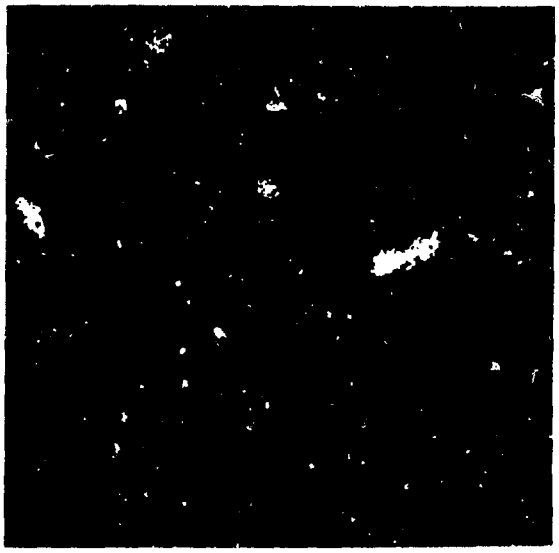

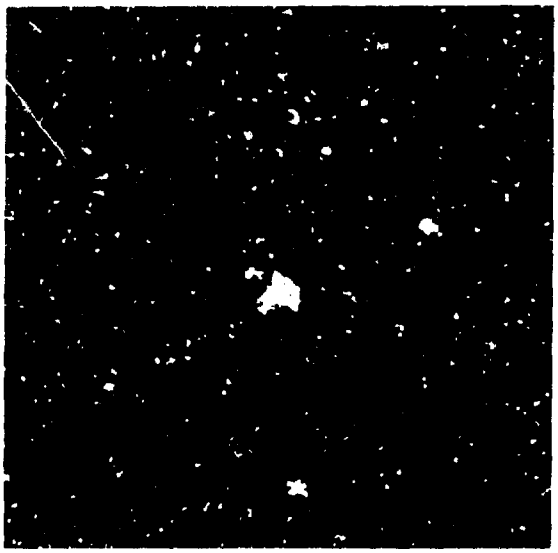

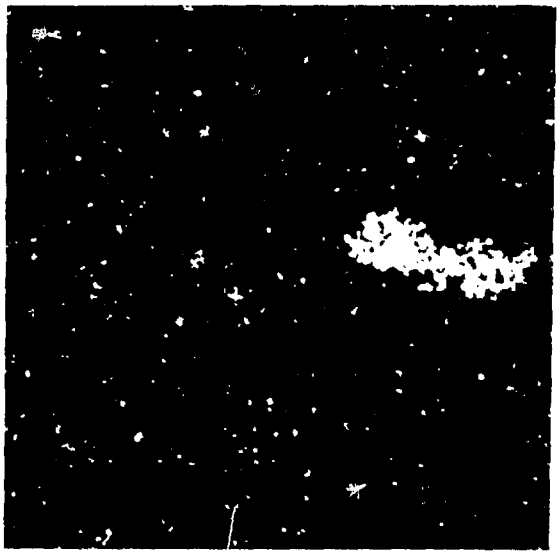

Fig. 2. Powder TaC-29, nominal 1.3-μm average particle size. (Conventional metallography. Top, 100X. Bottom, 250X.)

Fig. 3. Powder TaC-30, nominal 1.37-μm average particle size. (Conventional metallography. Top, 100X. Bottom, 250X.)

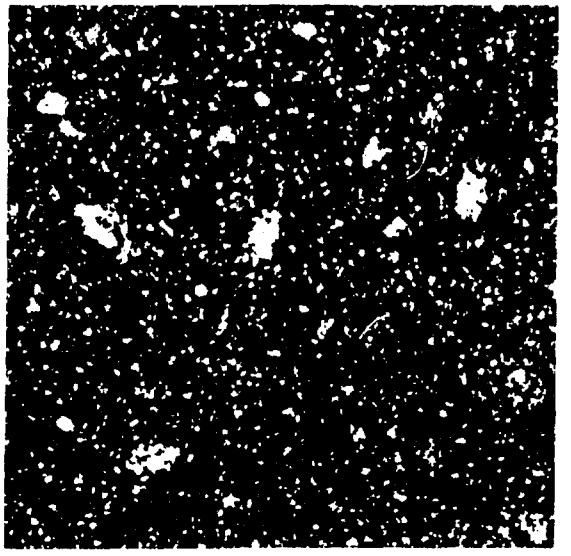

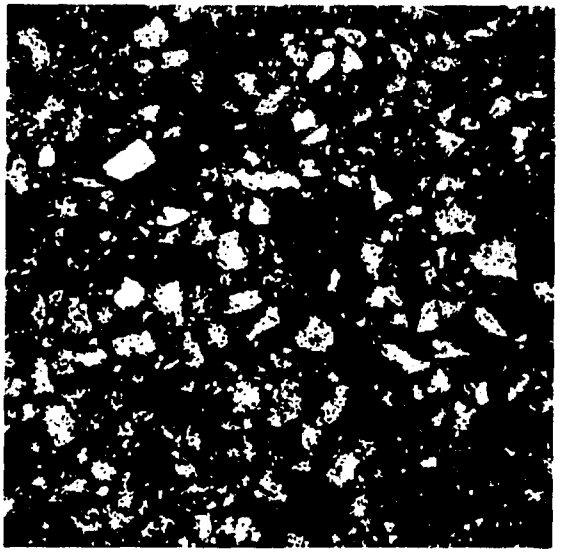

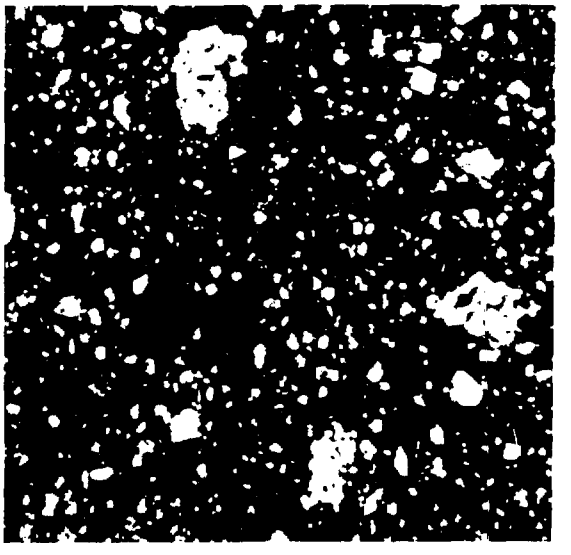

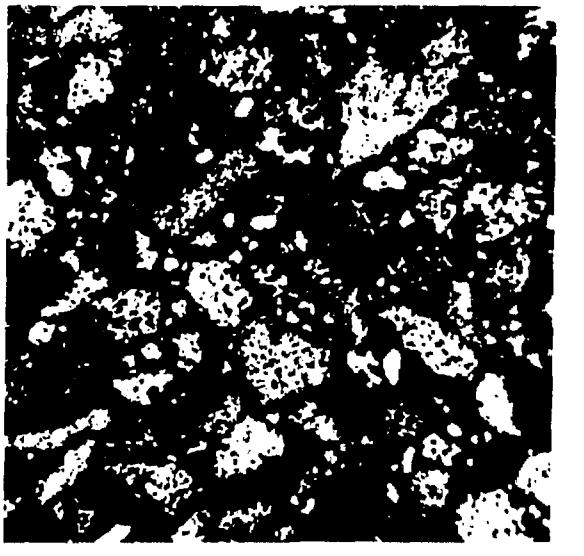

Fig. 4. Powder TaC-32, nominal 1.85-μm average particle size. (Conventional metallography. Top, 100X. Bottom, 250X.)

Fig. 5. Powder TaC-45, nominal 8.6-μm average particle size. (Conventional metallography. Top, 100X. Bottom, 250X.)

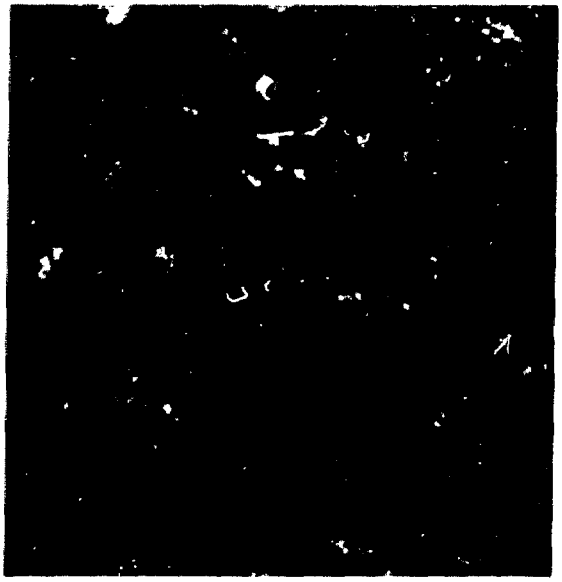

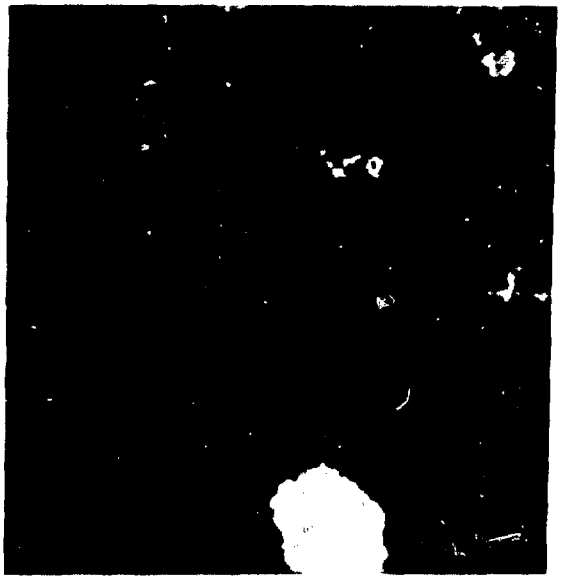

Fig. 6. Nominal 300-Å average particle size. (Scanning electron micrographs. Sample TaC-38. Top, 1000X. Bottom, 3000X.)

Fig. 7. Nominal 300-Å average particle size. (Scanning electron micrographs. Sample TaC-38. Top, 5000X. Bottom, 5000X.)

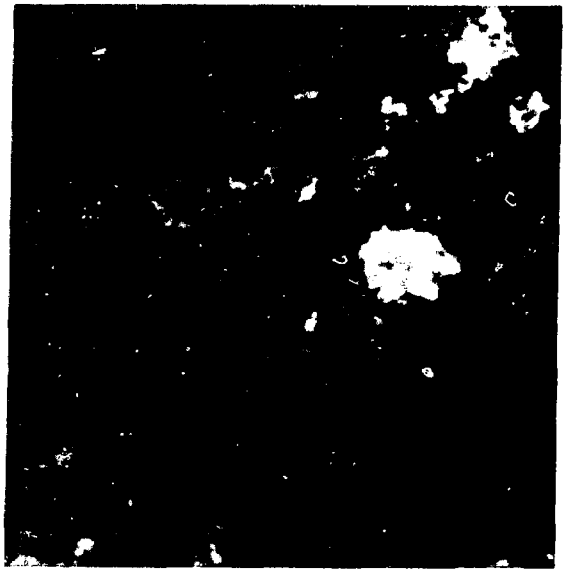

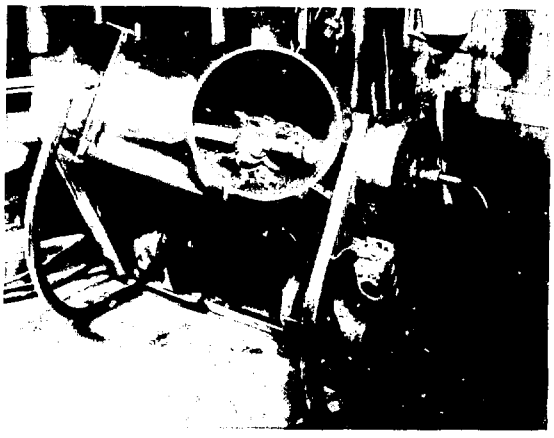

Fig. 9. Patterson-Kelly 16-qt twin shell blender.

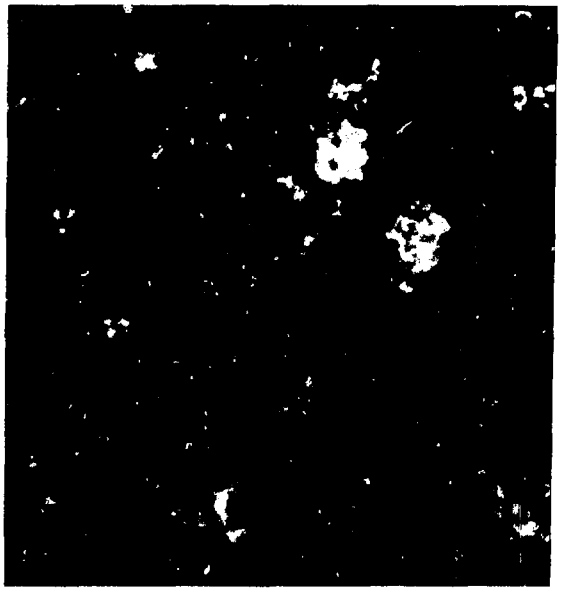

Fig. 8. Nominal 300-Å average particle size. (Scanning electron micrographs. Sample TaC-38. 10,000X.)

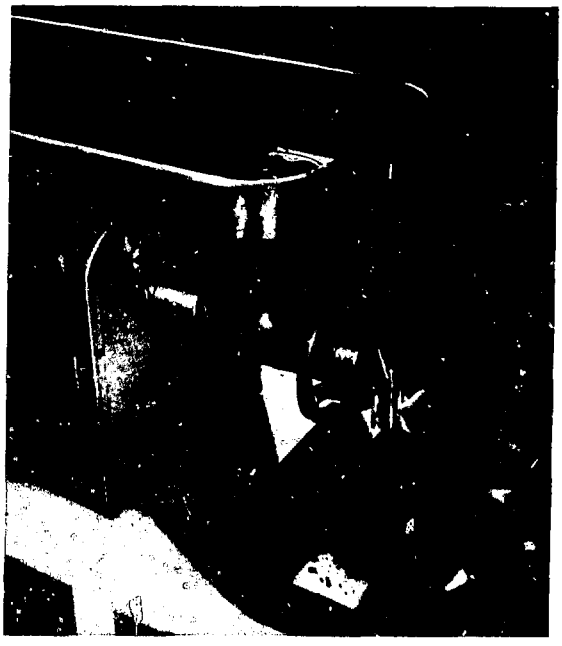

Fig. 10. Hobart chopper with mix.

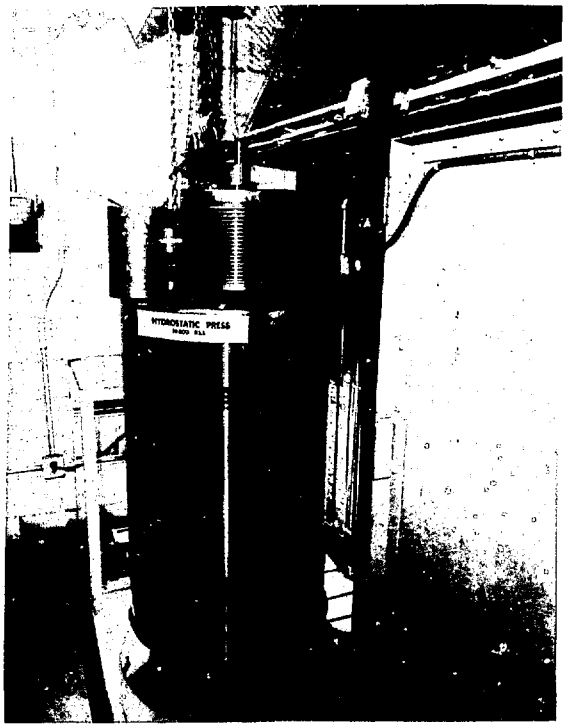

Fig. 11. Hydrostatic press.

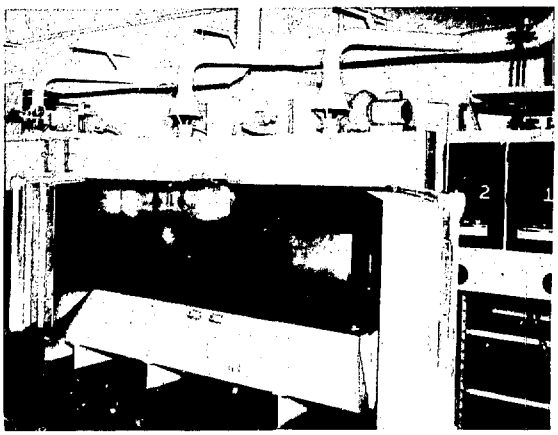

Fig. 12. Curing oven.

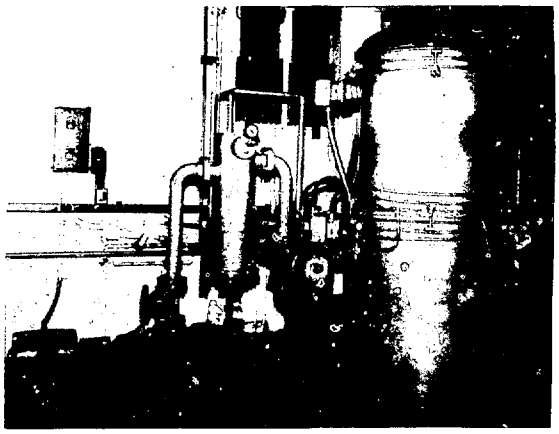

Fig. 13. Baking furnace.

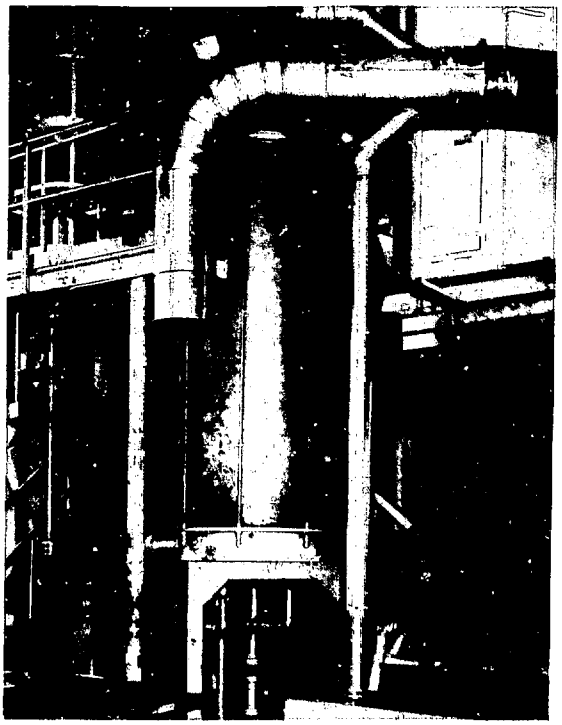

Fig. 14. Sintering furnace.

Fig. 15. High-temperature sintering furnace.

Fig. 16. Hot-pressing furnaces.

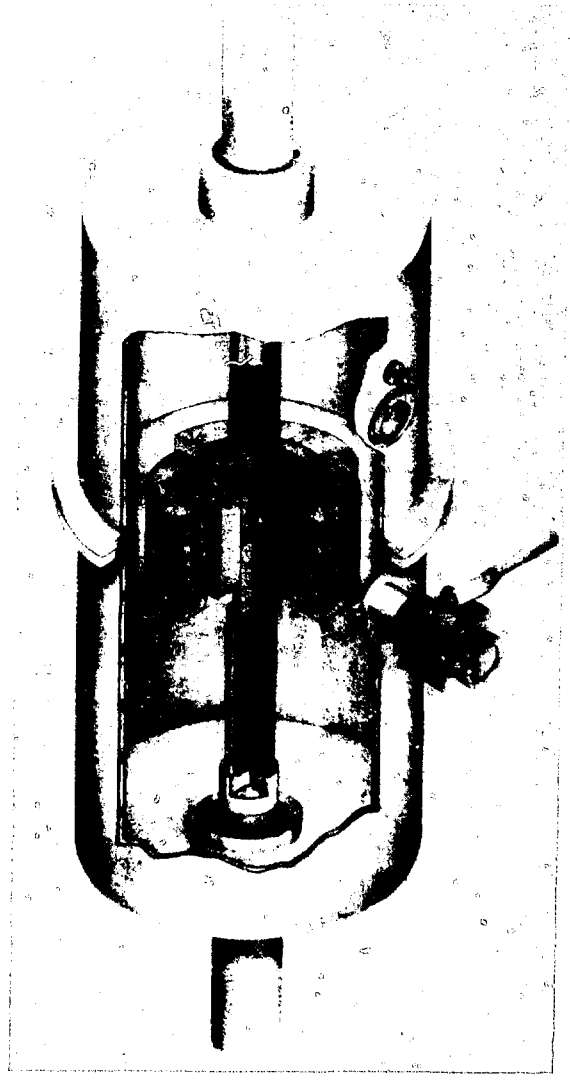

Fig. 17. Schematic drawing of hot-pressing furnace.

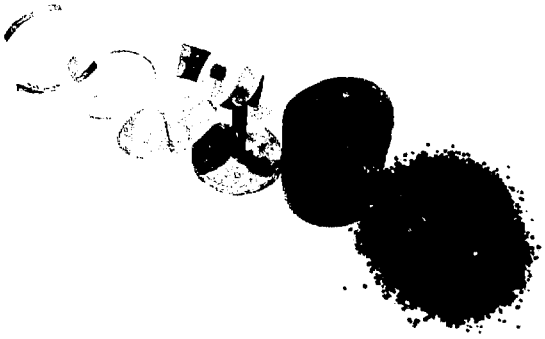

Fig. 18. Pressing sack components: (left to right) Aero seal clamp, clamping ring, lid with hypodermic needle penetrating into sponge, tamper, sack, and mix.

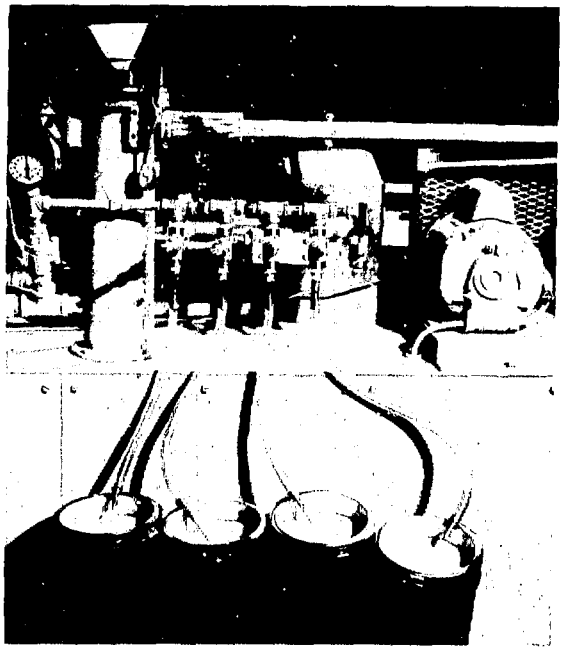

Fig. 19. Evacuation of pressing sacks.

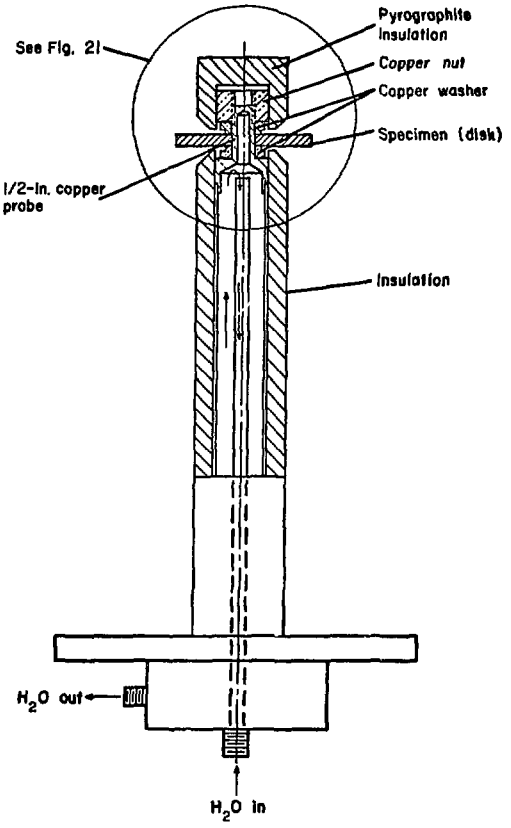

Fig. 20. Steady-state thermal stress test rig.

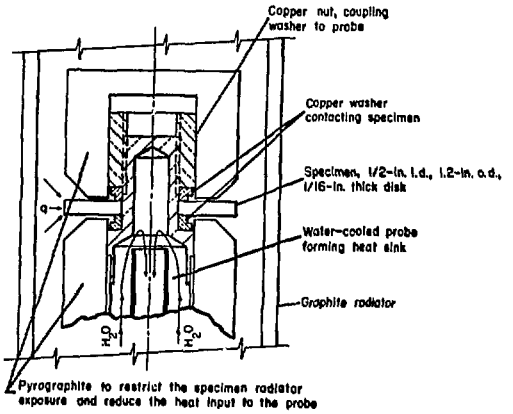

Fig. 21. Enlargement of part of Fig. 20.

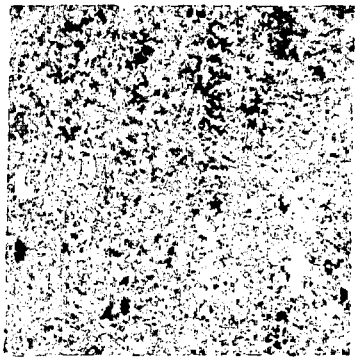

(a) 100X.

(a) 250X.

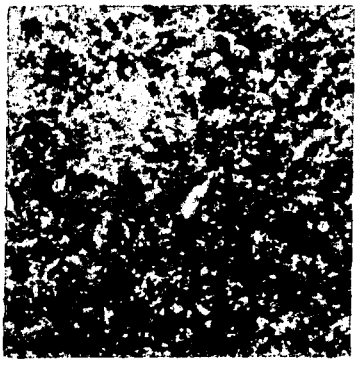

(b) 100X.

(b) 250X.

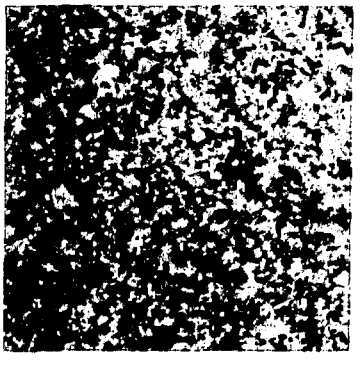

(c) 100X.

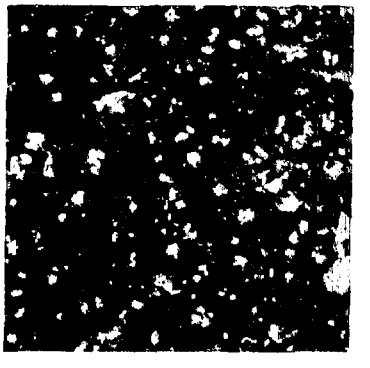

(c) 250X.

Fig. 22. Microstructure showing the distribution in a graphite matrix of TaC with an APS of (a) ~ 300 Å, (b) 0.13 μm, and (c) 4.2 μm.

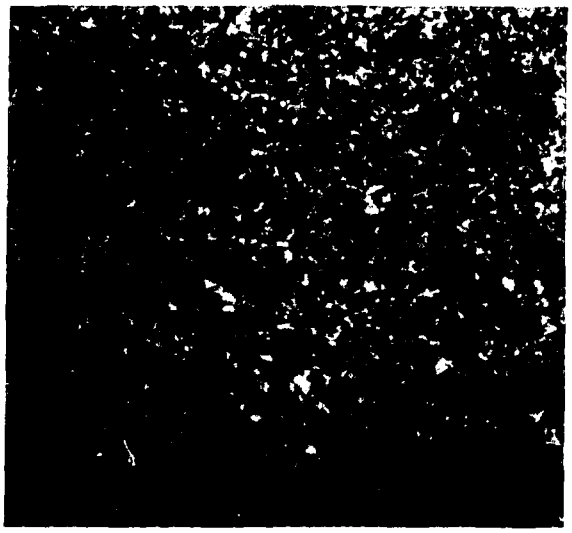

Fig. 23. Structure of 40 wt%(10 vol%) TaC (~300 Å)-carbon composite. (Scanning electron micrographs. Top, 100X. Bottom left, 300X. Bottom right, 500X.)

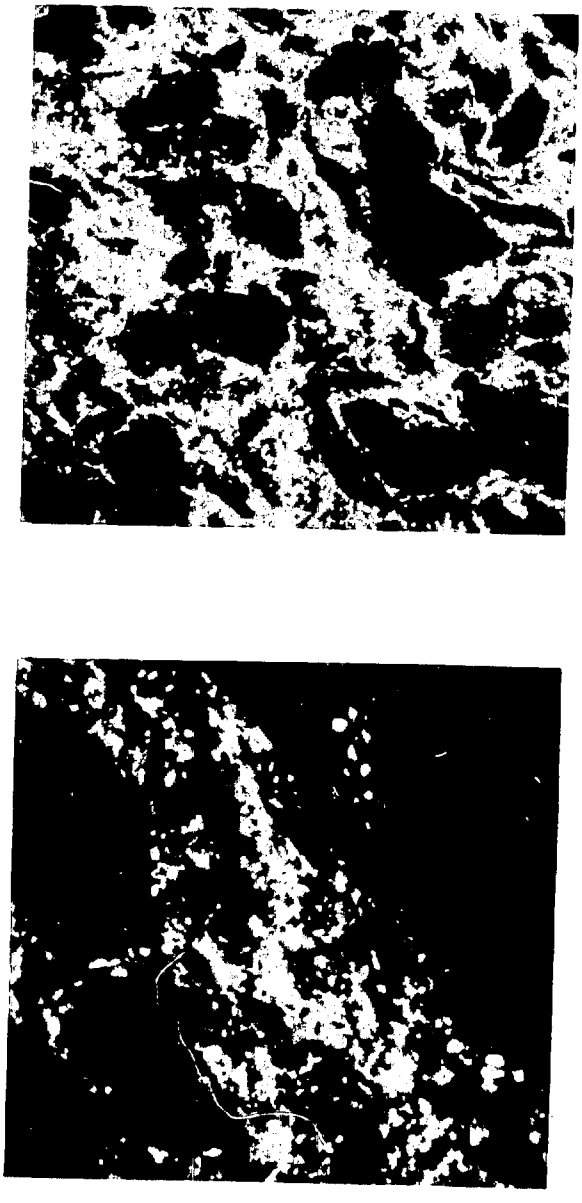

Fig. 24. Structure of 40 wt%(10 vol%) TaC (300 Å)-carbon composite. (Scanning electron micrographs. Top, 1000X. Bottom, 3000X.)

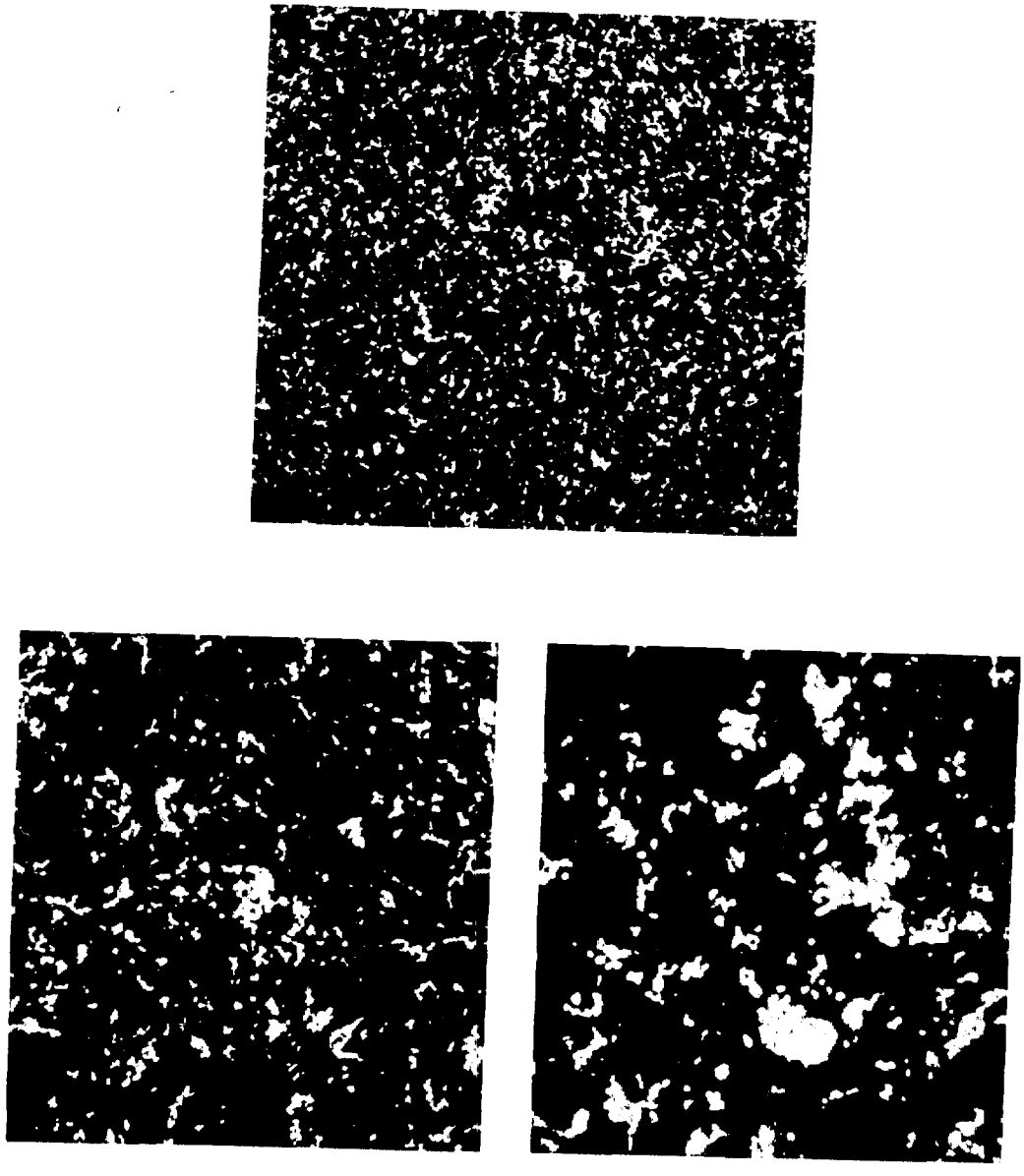

Fig. 25. Structure of 40 wt%(10 vol%) TaC (0.13 μm)-carbon composite. (Scanning electron micrographs. Top, 100X. Bottom left, 300X. Bottom right, 500X.)

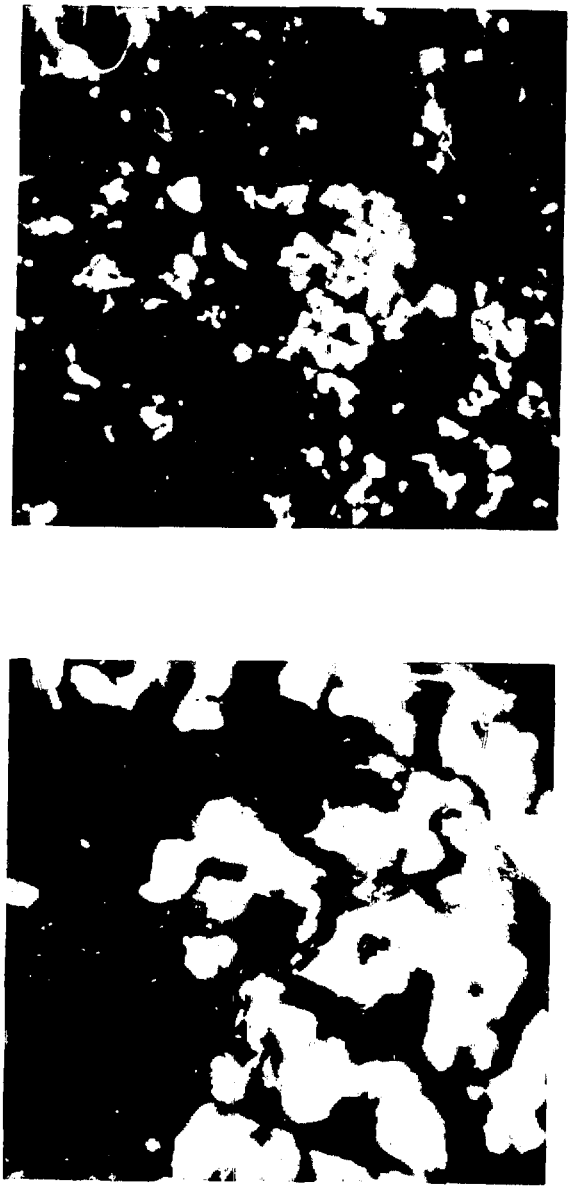

Fig. 26. Structure of 40 wt%(10 vol%) TaC (0.13 μm)-carbon composite. (Scanning electron micrographs. Top, 1000X. Bottom, 3000X.)

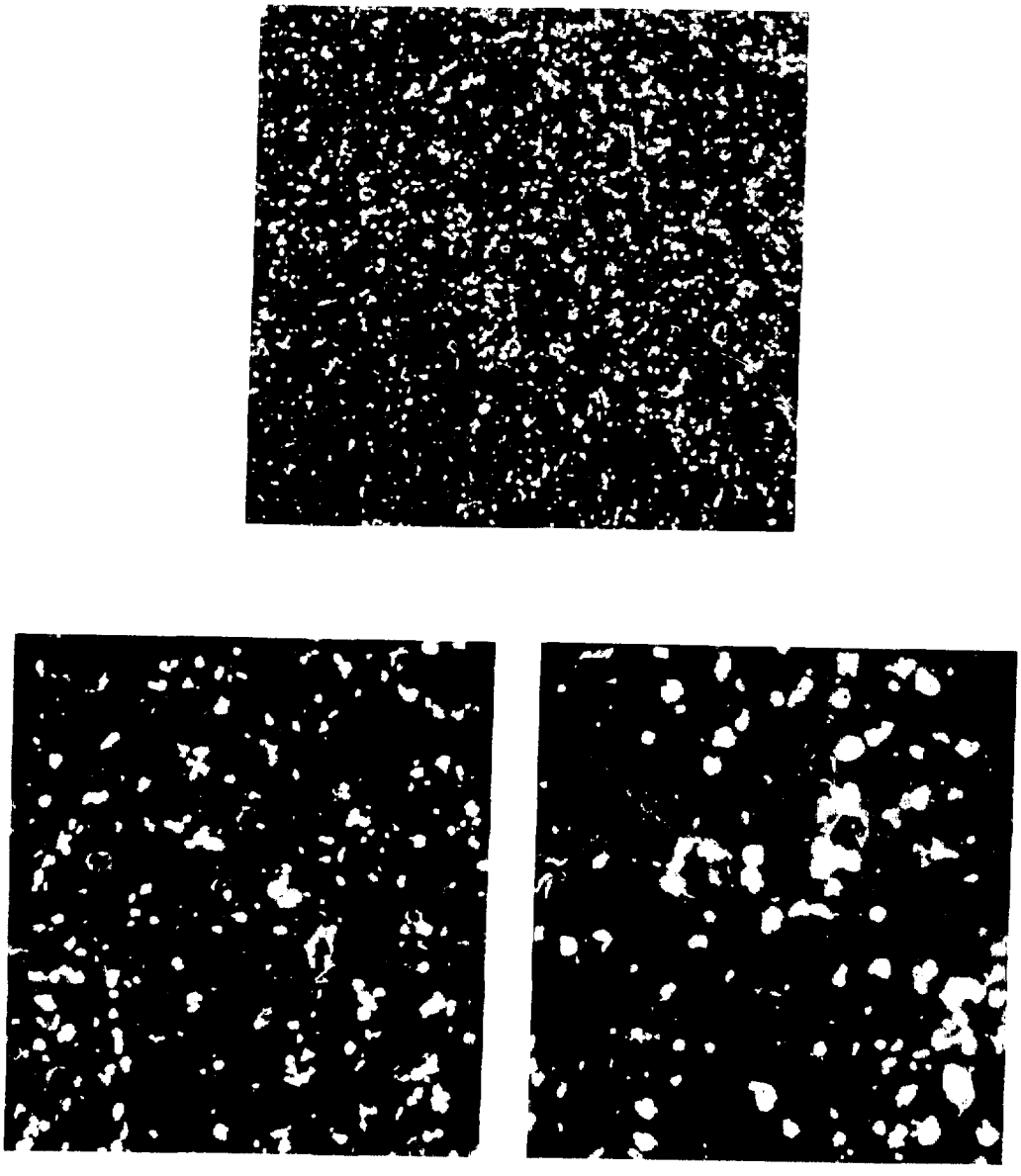

Fig. 27. Structure of 40 wt%(10 vol%) TaC (4.2 μm)-carbon composite. (Scanning electron micrographs. Top, 100X. Bottom left, 300X. Bottom right, 500X.)

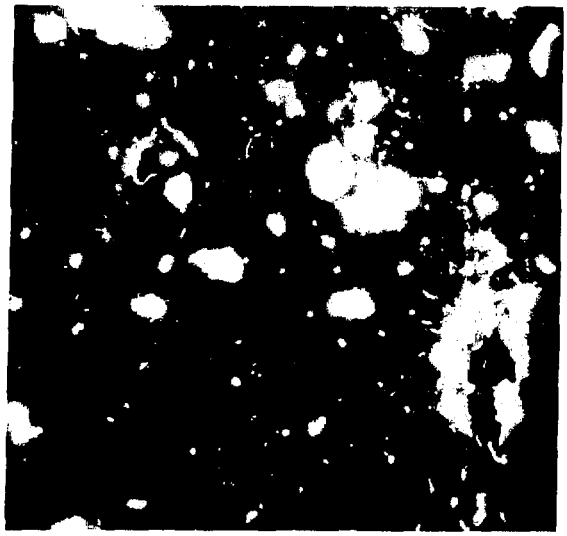

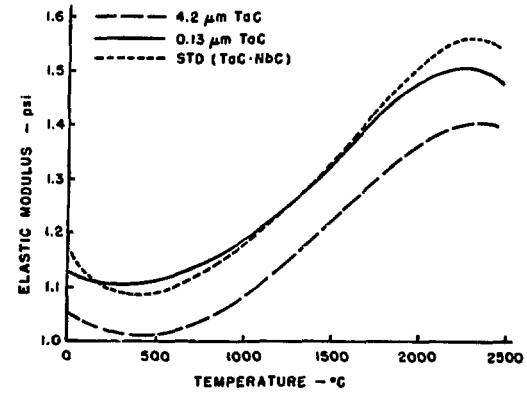

Fig. 29. Dynamic elastic modulus vs temperature.

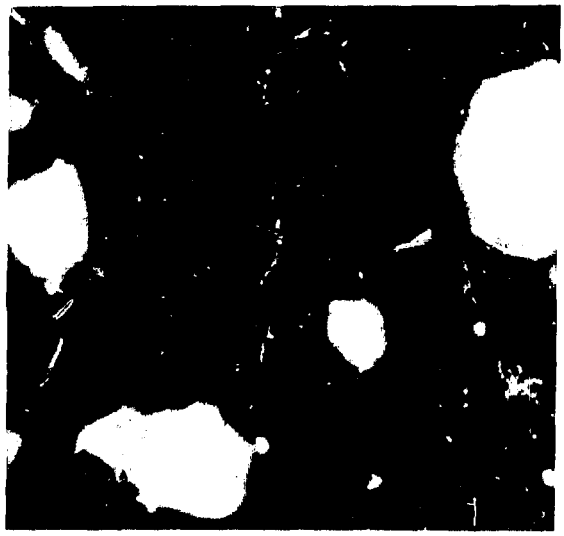

Fig. 28. Structure of 40 wt%(10 vol%) TaC (4.2 μm)-carbon composite. (Scanning electron micrographs. Top, 1000X. Bottom, 3000X.)

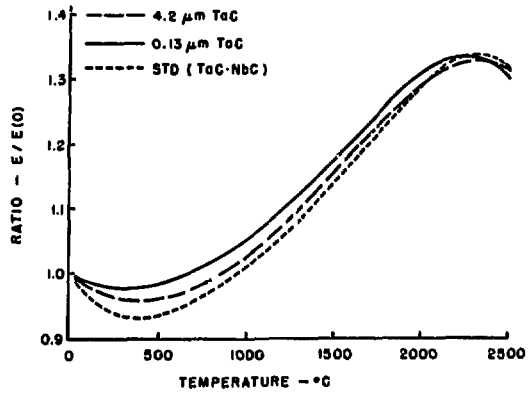

Fig. 30. Reduced elastic modulus.

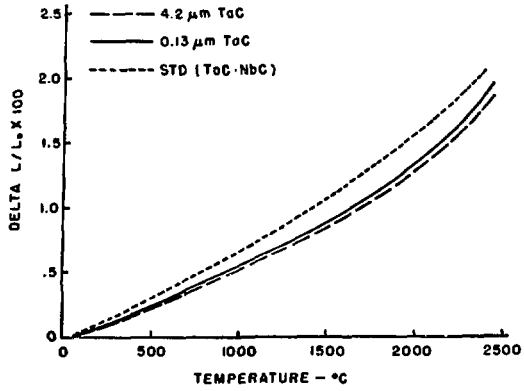

Fig. 31. Thermal expansion vs temperature.

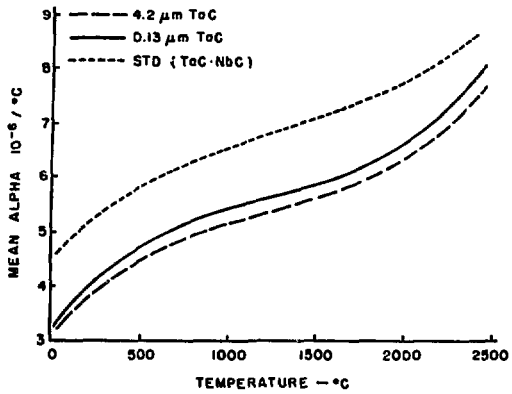

Fig. 32. Mean coefficient of thermal expansion.

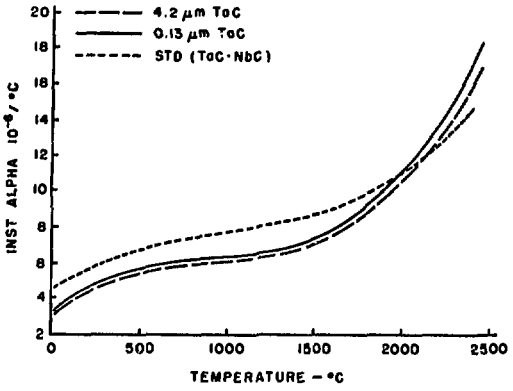

Fig. 33. Instantaneous coefficient of thermal expansion.

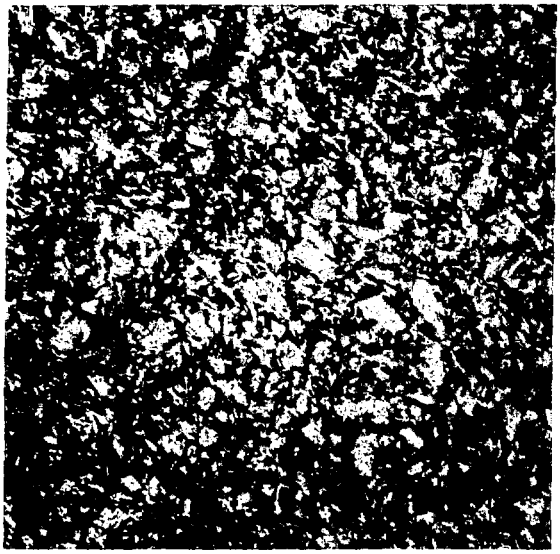

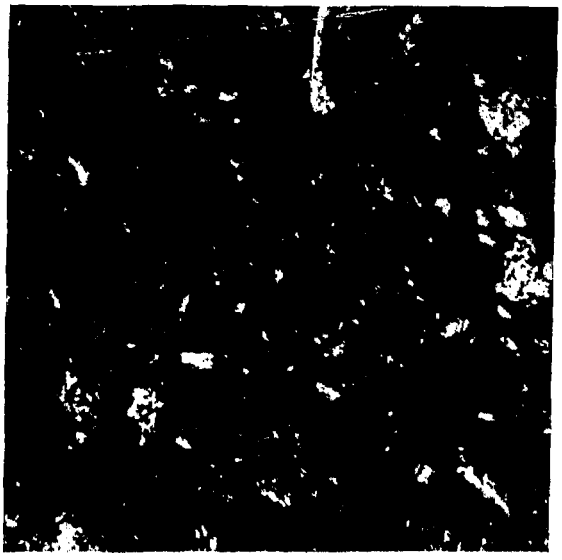

Fig. 34. Microstructure of graphite specimen containing -325 mesh M-3 graphite.

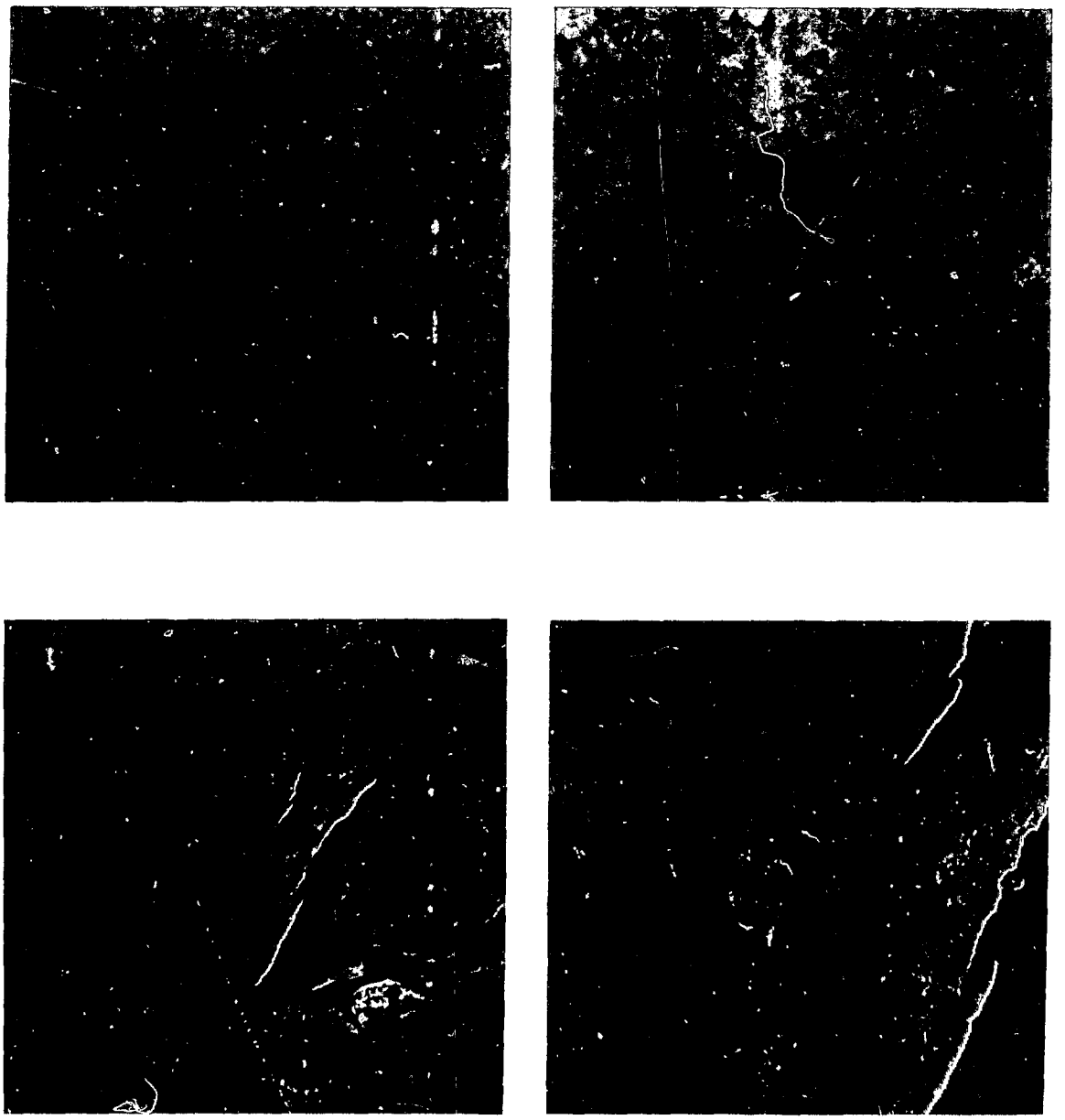

Fig. 35. Microstructure of graphite sample containing -325 mesh M-3 graphite flour. (Scanning electron micrographs. Top left, 100X. Top right, 300X. Bottom left, 1000X. Bottom right, 3000X.)

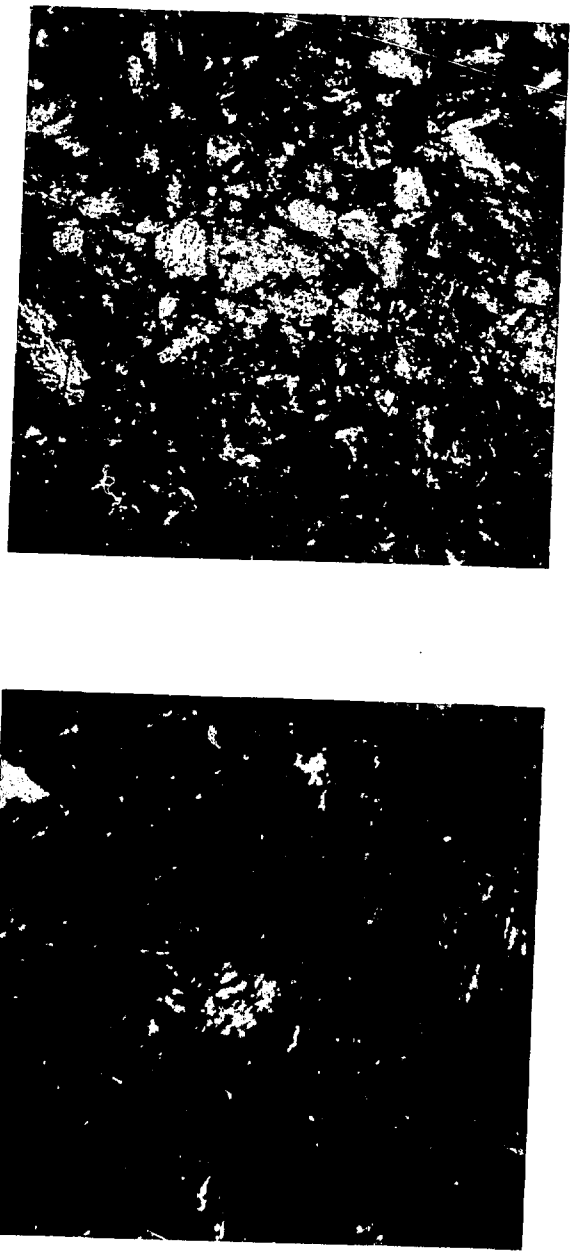

Fig. 36. Microstructure of graphite specimen containing 85 wt% M-3 graphite flour and 15 wt% Thermax. (Conventional metallography. Top, 100X. Bottom, 500X.)

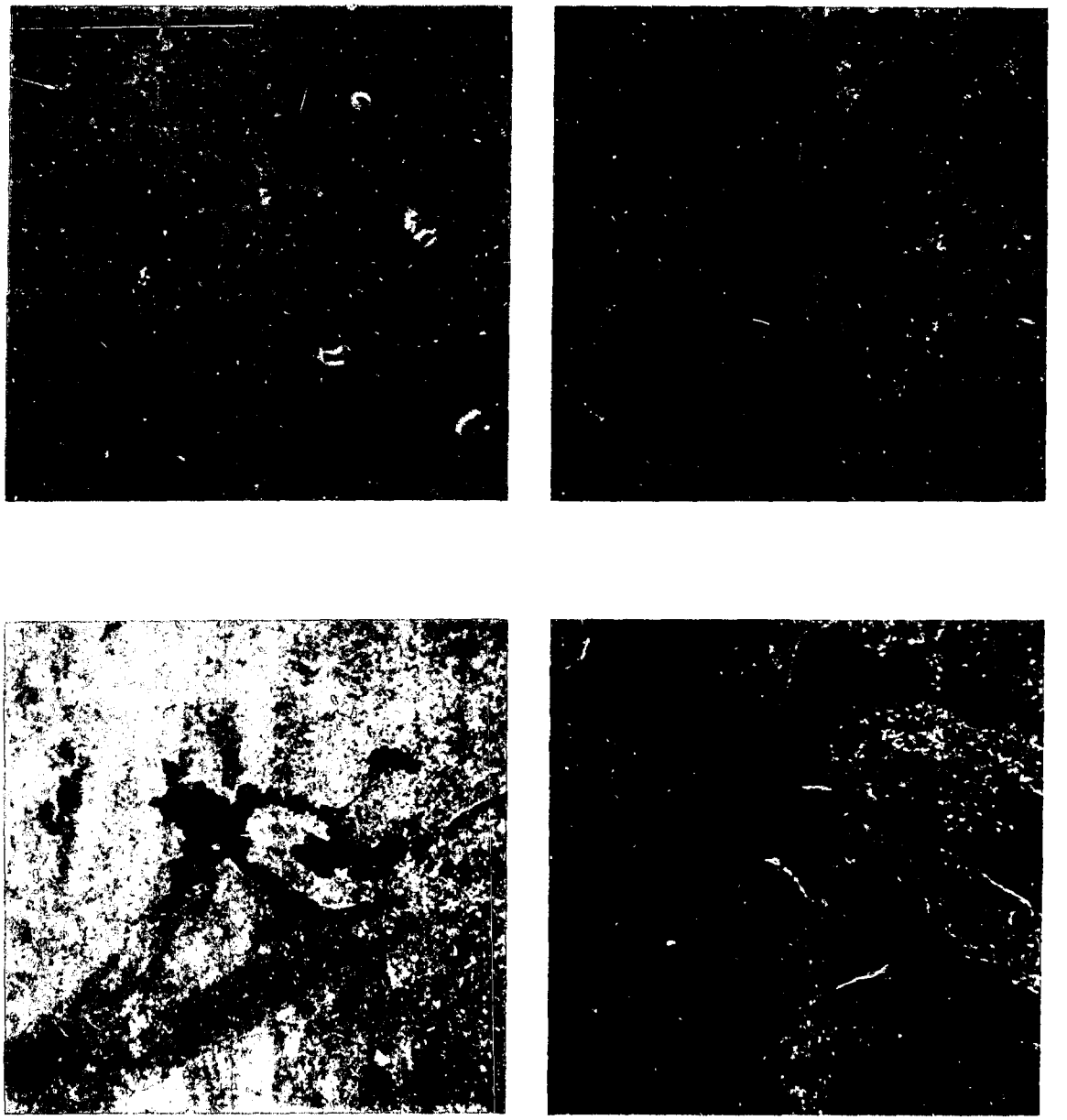

Fig. 37. Microstructure of graphite sample containing 85 wt% M-3 graphite flour and 15 wt% Thermax. (Scanning electron micrographs. Top left, 100X. Top right, 300X. Bottom left, 1000X. Bottom right, 3000X.)

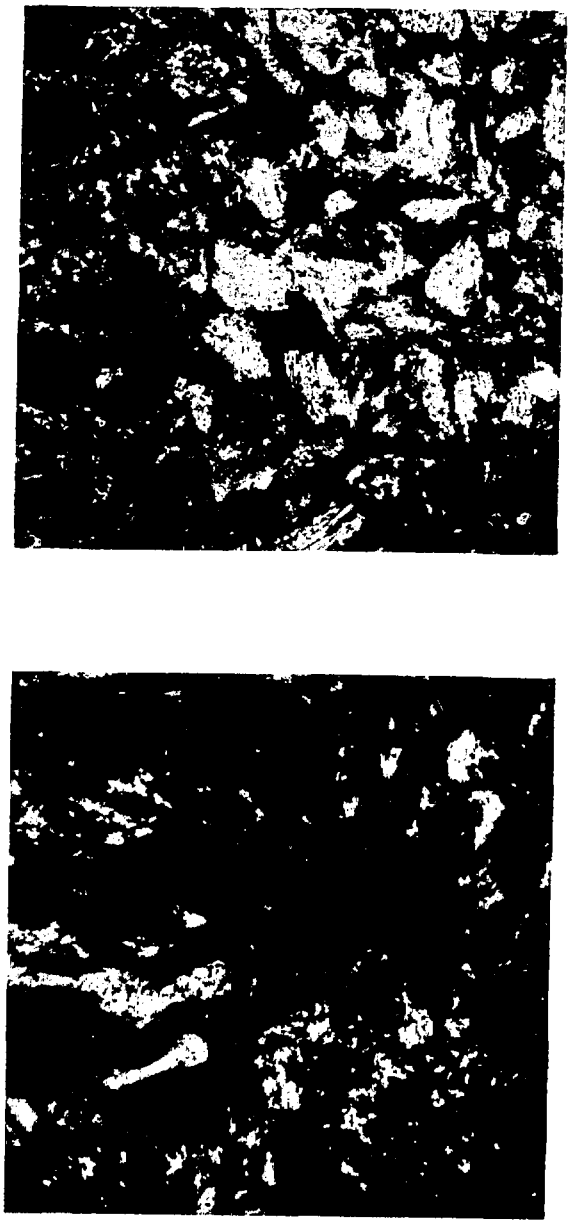

Fig. 38. Microstructure of graphite specimen containing -150 +325 mesh M-3 graphite flour. (Conventional metallography. Top, 100X. Bottom, 500X.)

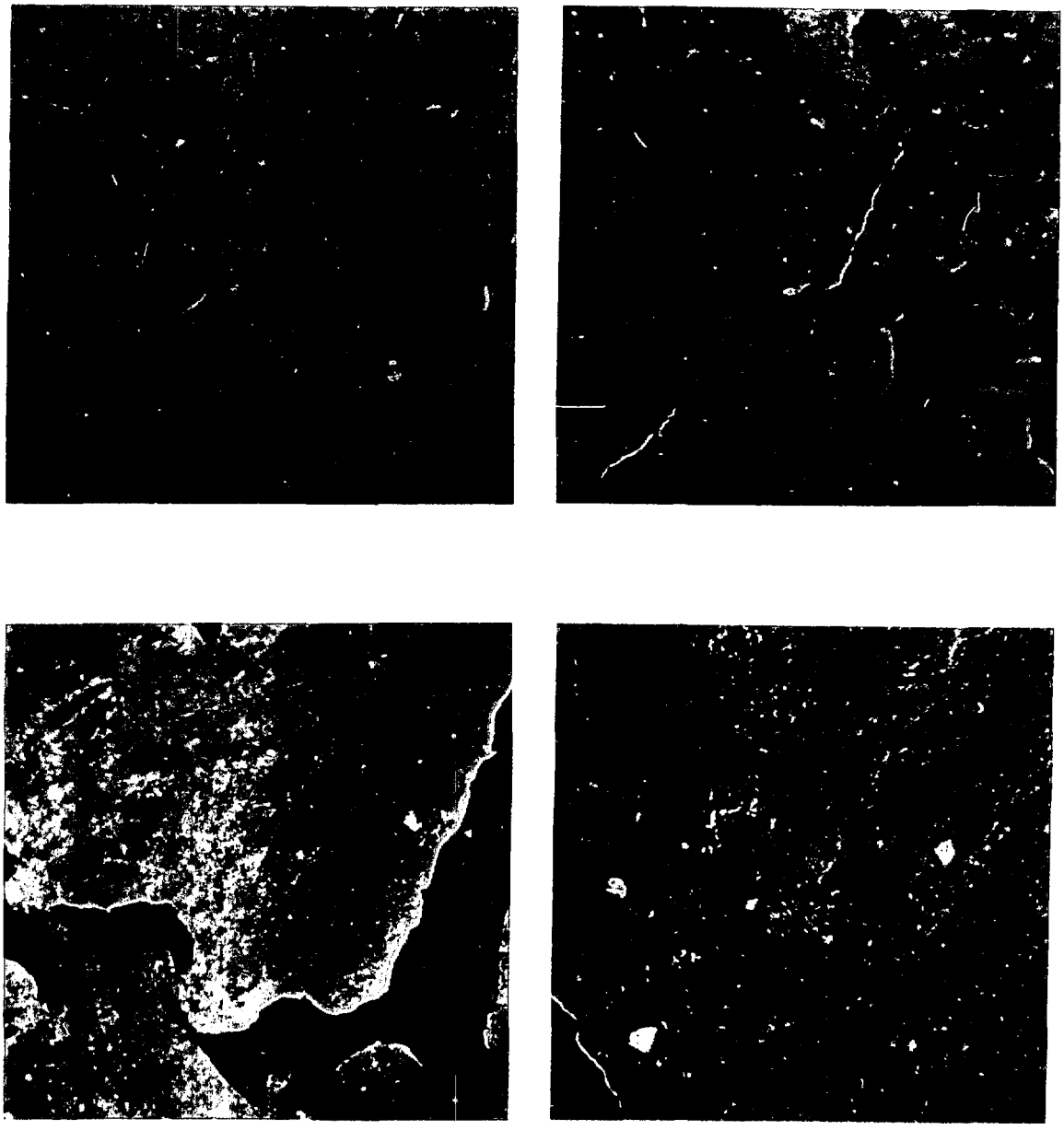

Fig. 39. Microstructure of graphite sample containing -150 +325 mesh M-3 graphite flour. (Scanning electron micrographs. Top left, 100X. Top right, 300X. Bottom left, 1000X. Bottom right, 3000X.)

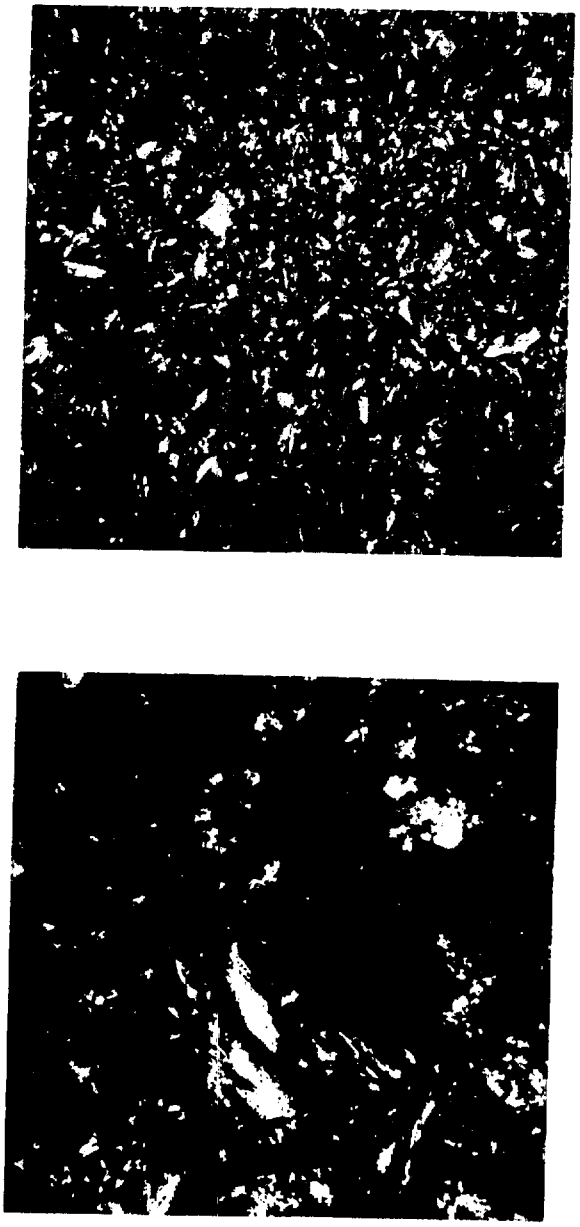

Fig. 40. Microstructure of TaC-C composite containing 1 wt% 300 Å TaC-38. (Conventional metallography. Top, 100X. Bottom, 500X.)

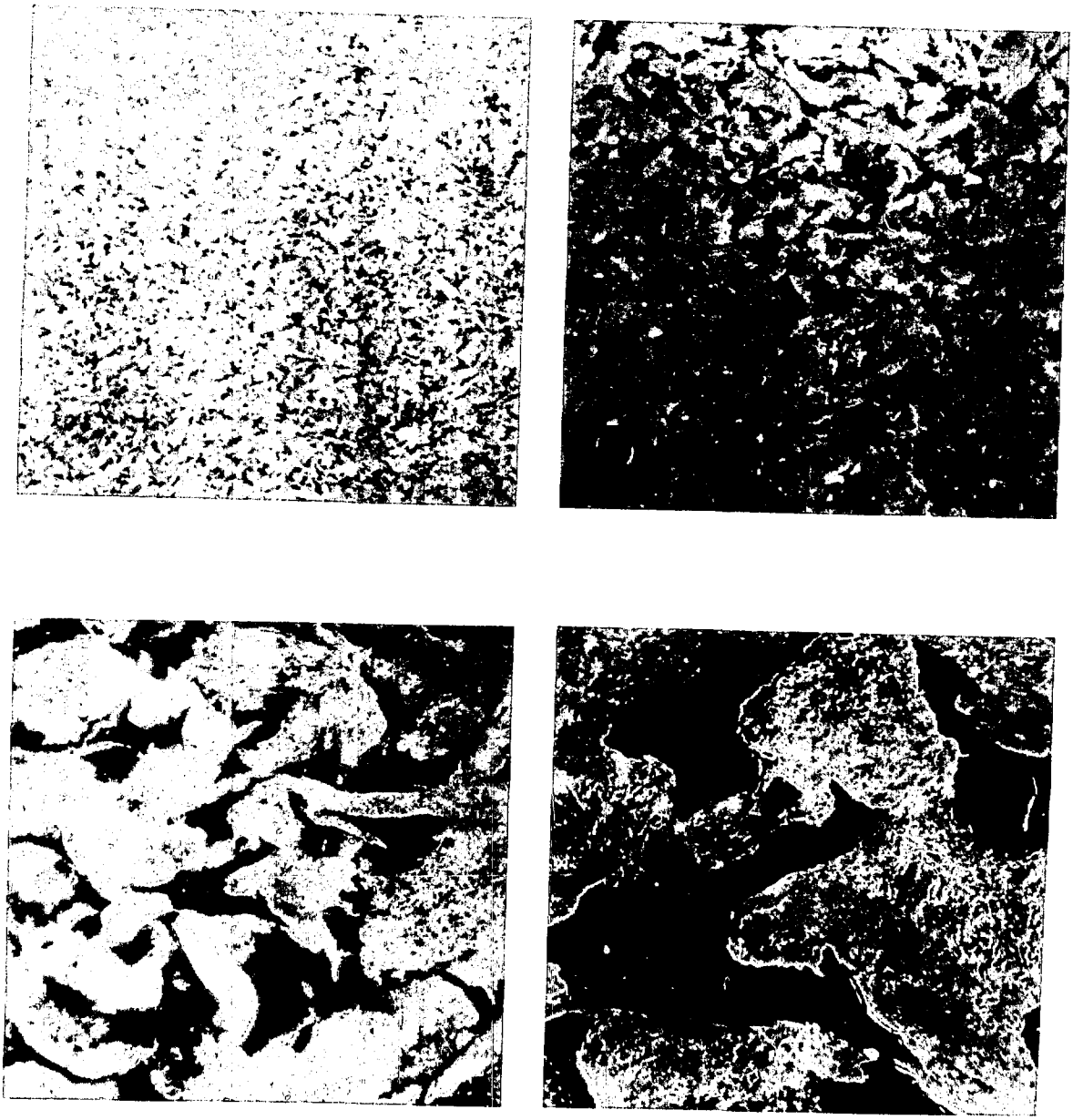

Fig. 41. Microstructure of TaC-C composite containing 1 wt% 300 Å TaC-38. (Scanning electron micrographs. Top left, 100X. Top right, 300X. Bottom left, 1000X. Bottom right, 3000X.)

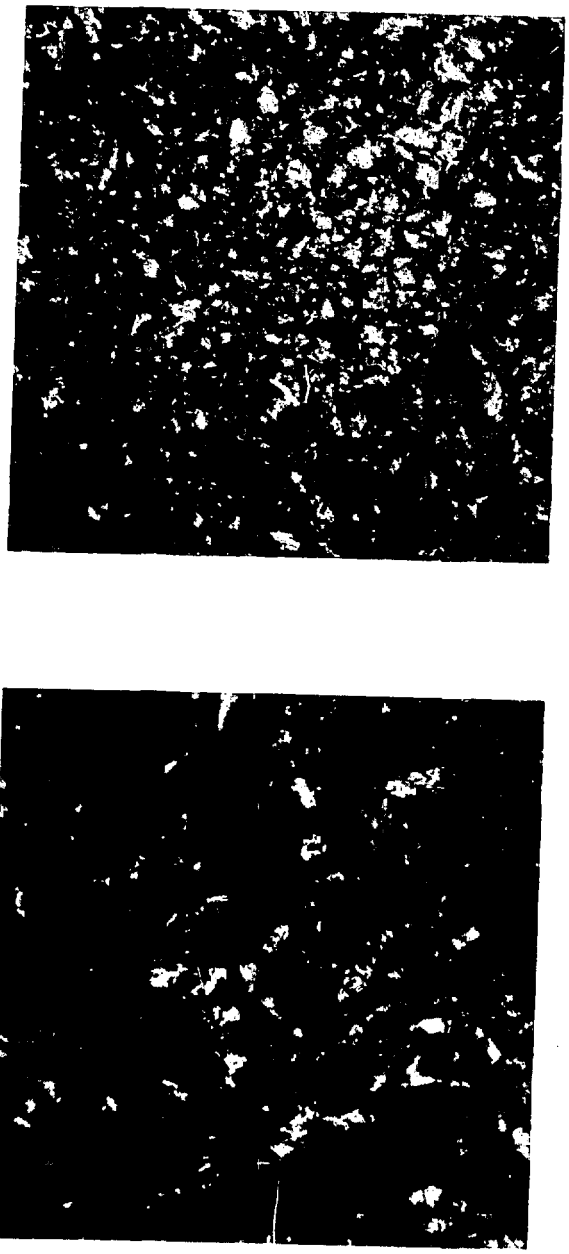

Fig. 42. Microstructure of TaC-C composite containing 5 wt% 300 Å TaC-38. (Conventional metallography. Top, 100X. Bottom, 500X.)

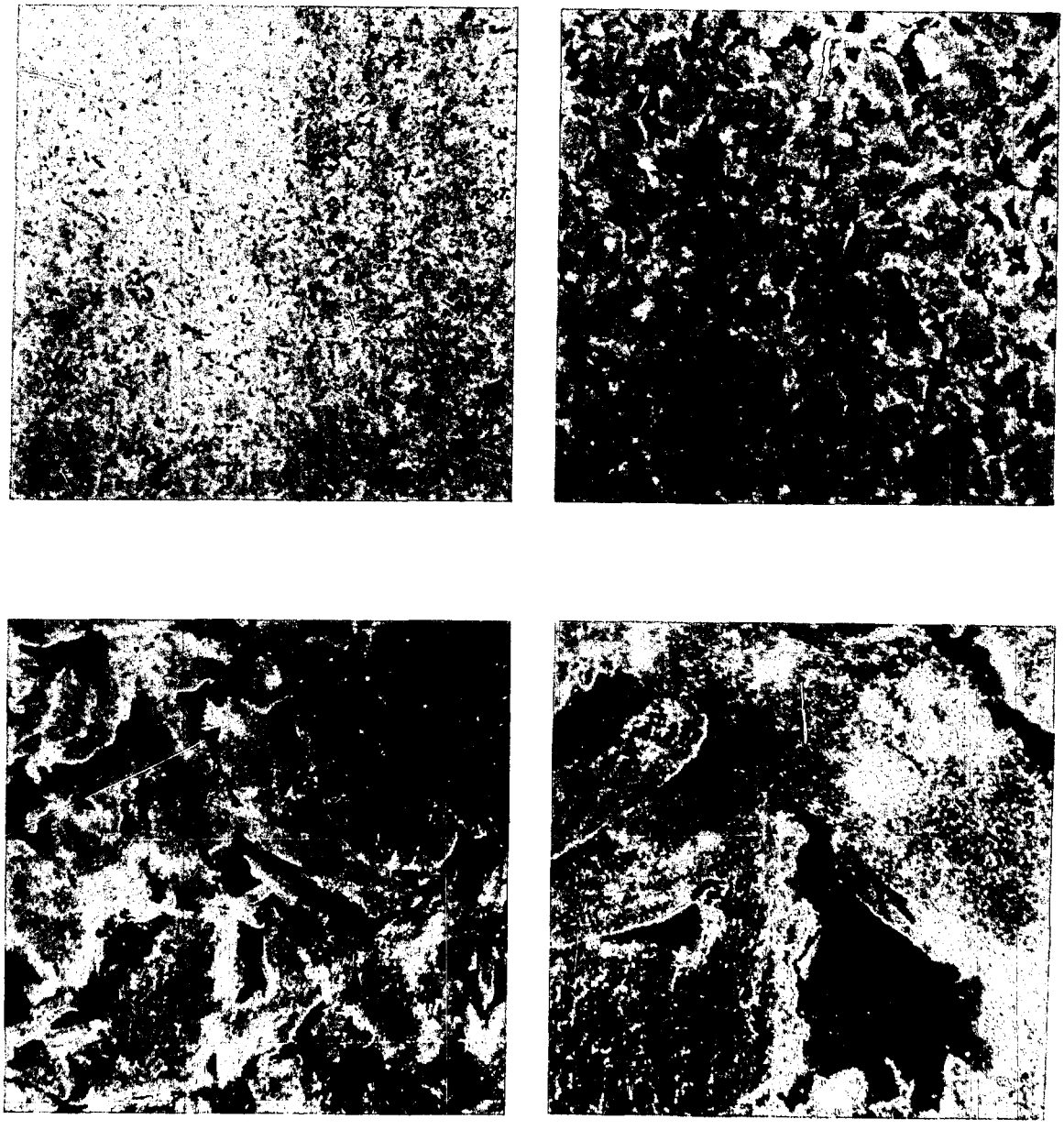

Fig. 43. Microstructure of TaC-C composite containing 5 wt% 300 Å TaC-38. (Scanning electron micrographs. Top left, 100X. Top right, 300X. Bottom left, 1000X. Bottom right, 3000X.)

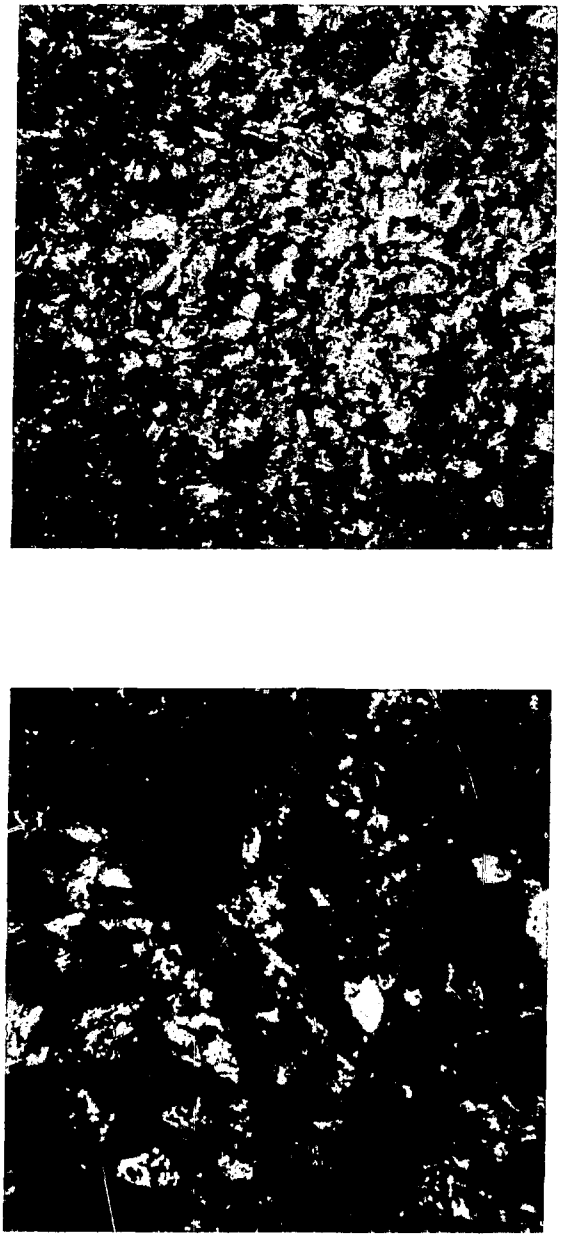

Fig. 44. Microstructure of TaC-C composite containing 7 wt% 300 Å TaC-38. (Conventional metallography. Top, 100X. Bottom, 500X.)

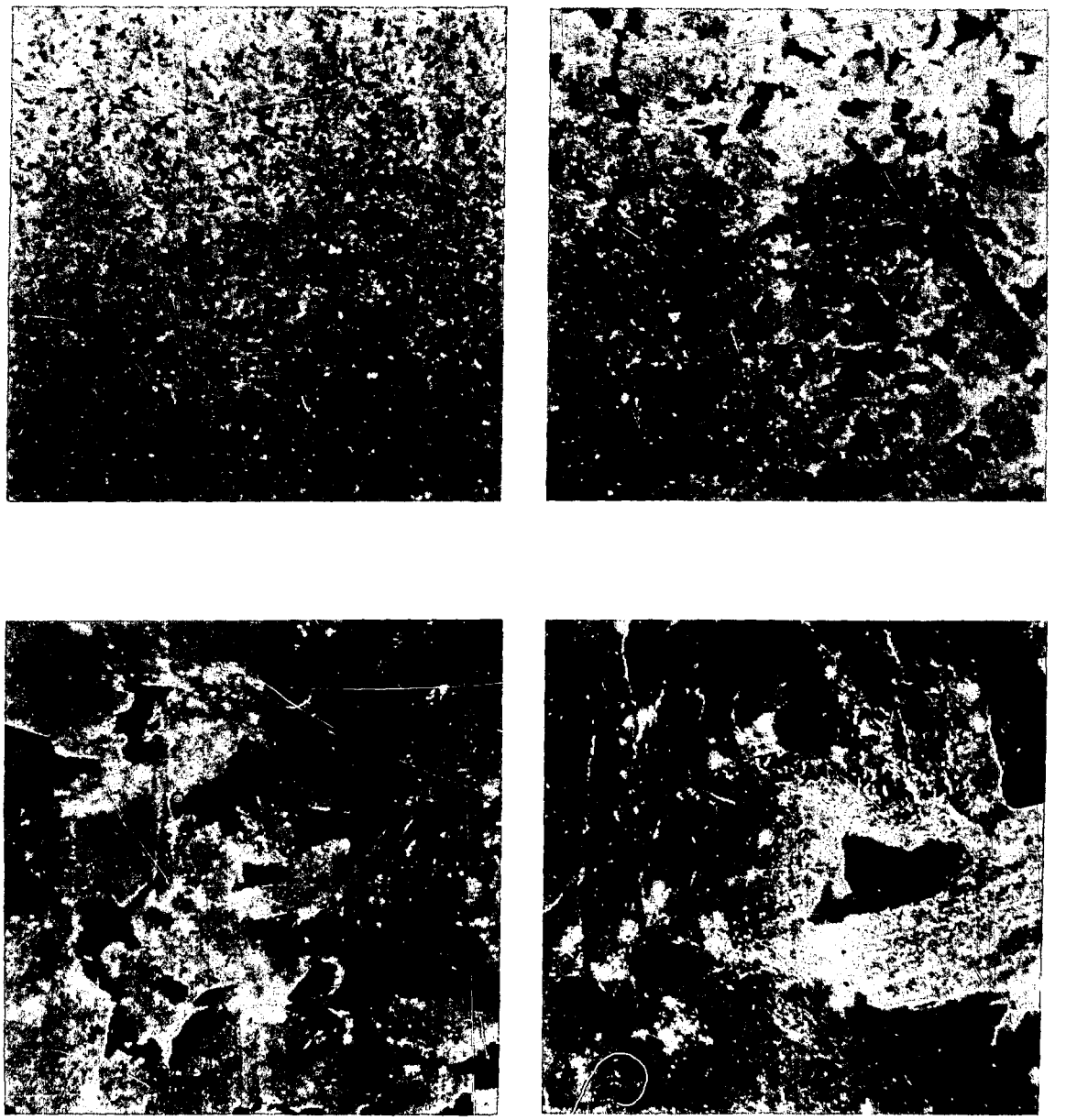

Fig. 45. Microstructure of TaC-C composite containing 7 wt% 300 Å TaC-38. (Scanning electron micrographs. Top left, 100X. Top right, 300X. Bottom left, 1000X. Bottom right, 3000X.)

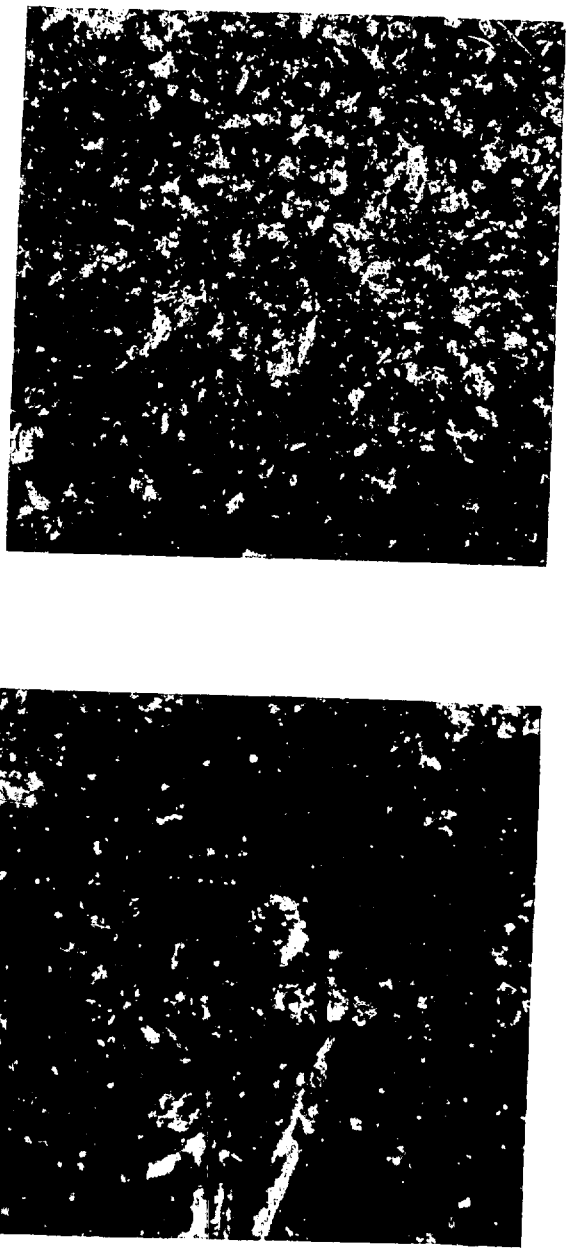

Fig. 46. Microstructure of TaC-C composite containing 14 wt% 300 Å TaC-38. (Conventional metallography. Top, 100X. Bottom, 500X.)

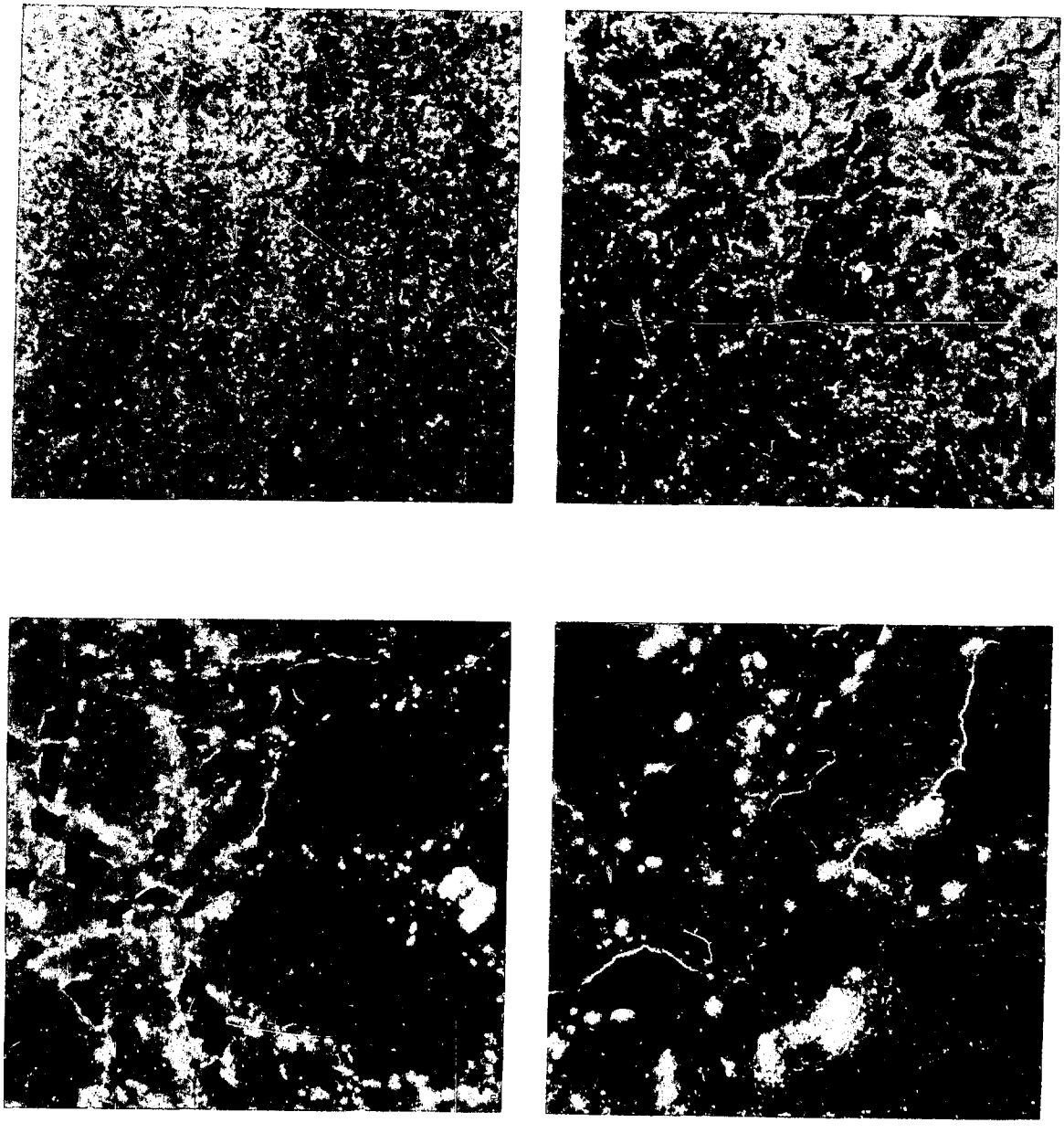

Fig. 47. Microstructure of TaC-C composite containing 14 wt% 300 Å TaC-38. (Scanning electron micrographs. Top left, 100X. Top right, 300X. Bottom left, 1000X. Bottom right, 3000X.)

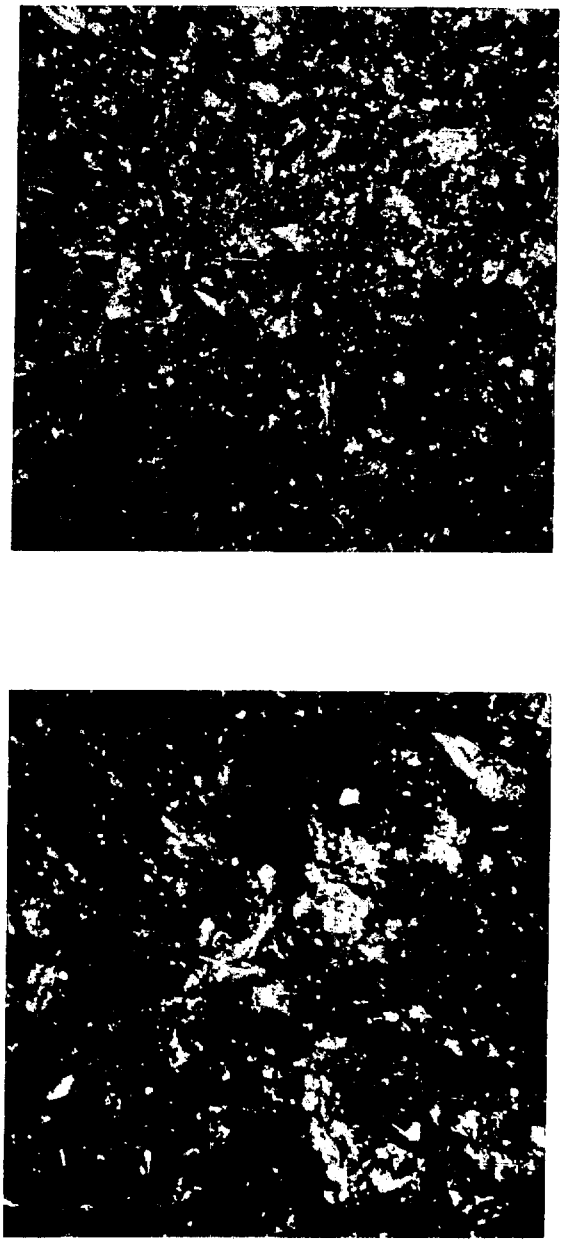

Fig. 48. Microstructure of TaC-C composite containing 20 wt% 300 Å TaC-38. (Conventional metallography. Top, 100X. Bottom, 500X.)

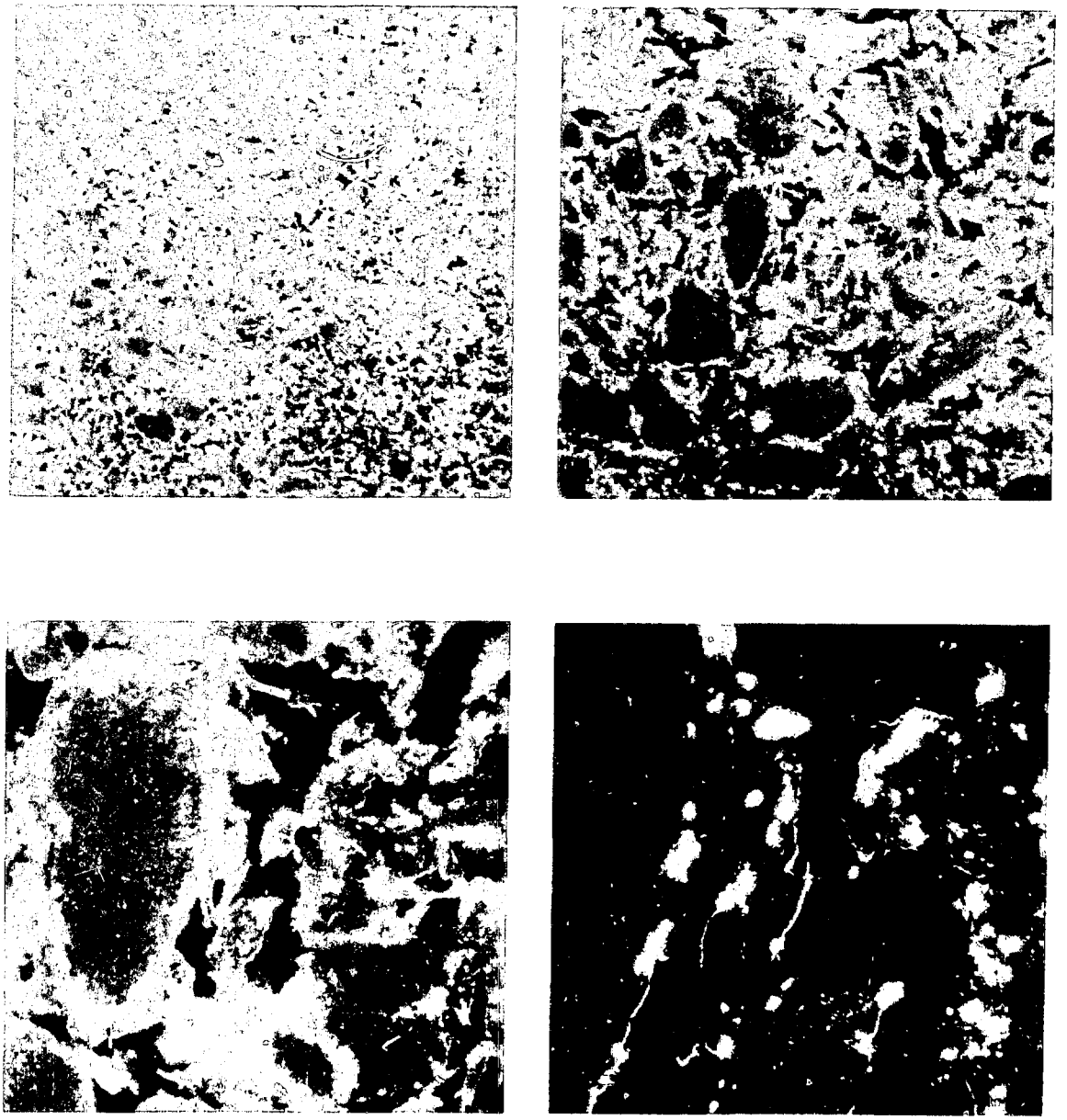

Fig. 49. Microstructure of TaC-C composite containing 20 wt% 300 Å TaC-38. (Scanning electron micrographs. Top left, 100X. Top right, 300X. Bottom left, 1000X. Bottom right, 3000X.)

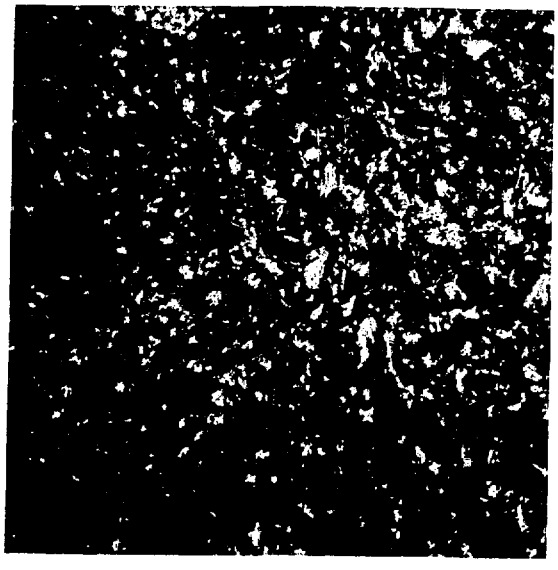

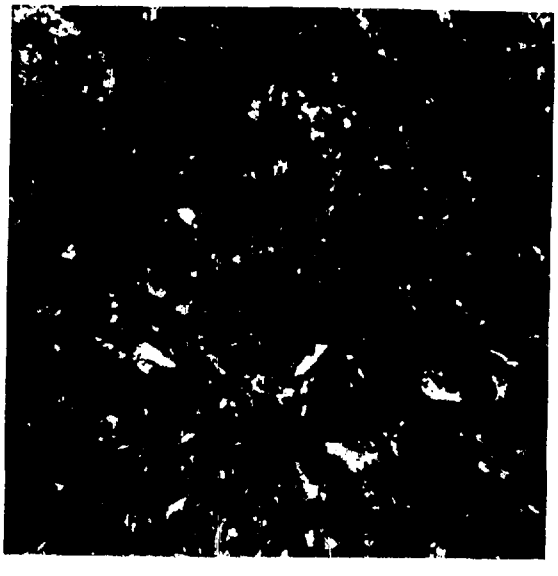

Fig. 50. Microstructure of TaC-C composite containing 1 wt% 1.3 μm TaC-30. (Conventional metallography. Top, 100X. Bottom, 500X.)

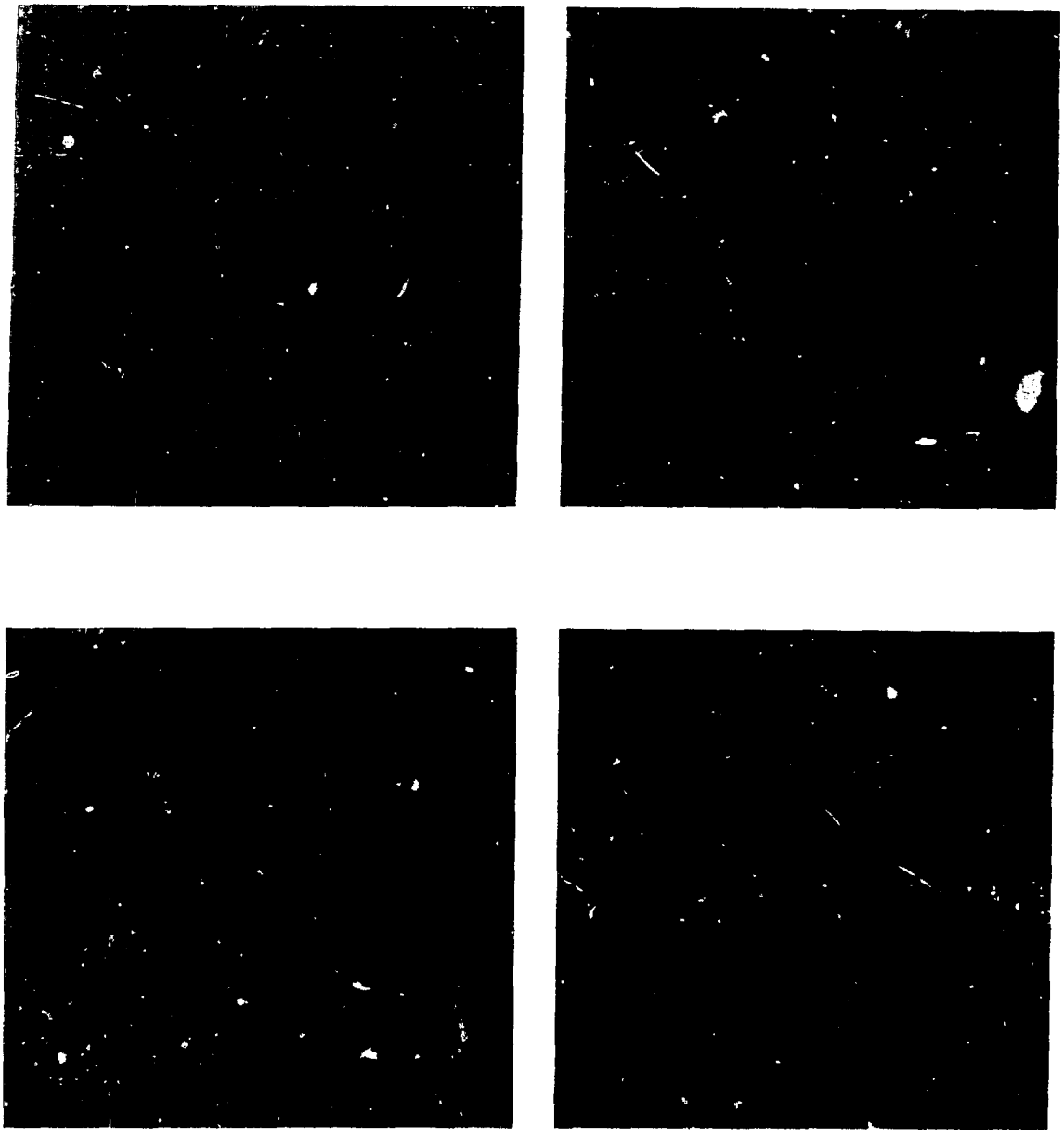

Fig. 51. Microstructure of TaC-C composite containing 1 wt% 1.3 μm TaC-30. (Scanning electron micrographs. Top left, 100X. Top right, 300X. Bottom left, 1000X. Bottom right, 3000X.)

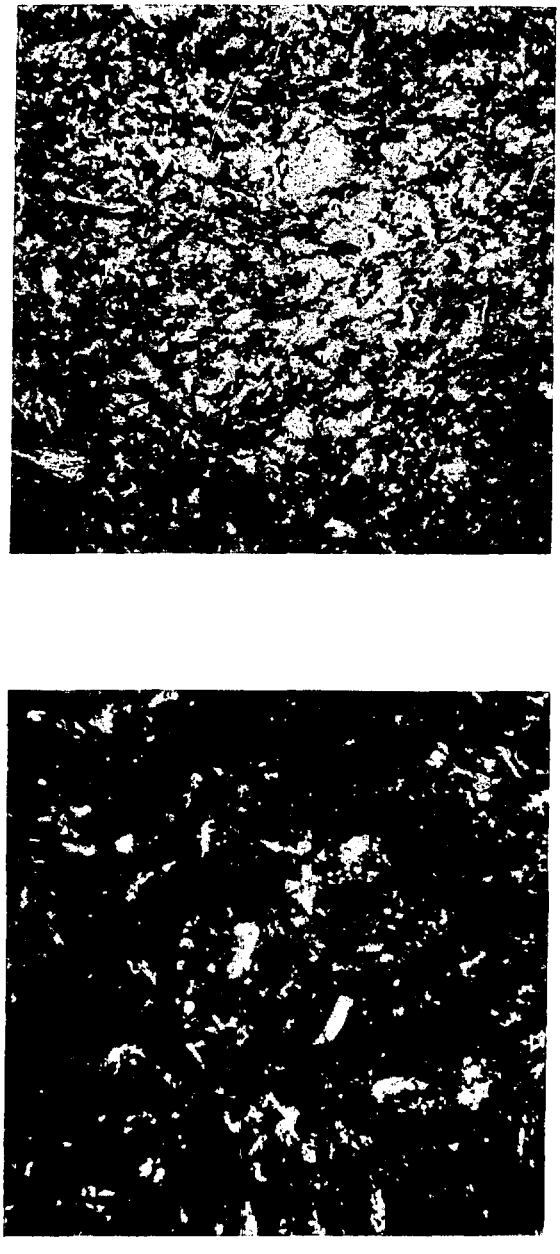

Fig. 52. Microstructure of TaC-C composite containing 5 wt% 1.3 μm TaC-30. (Conventional metallography. Top, 100X. Bottom, 500X.)

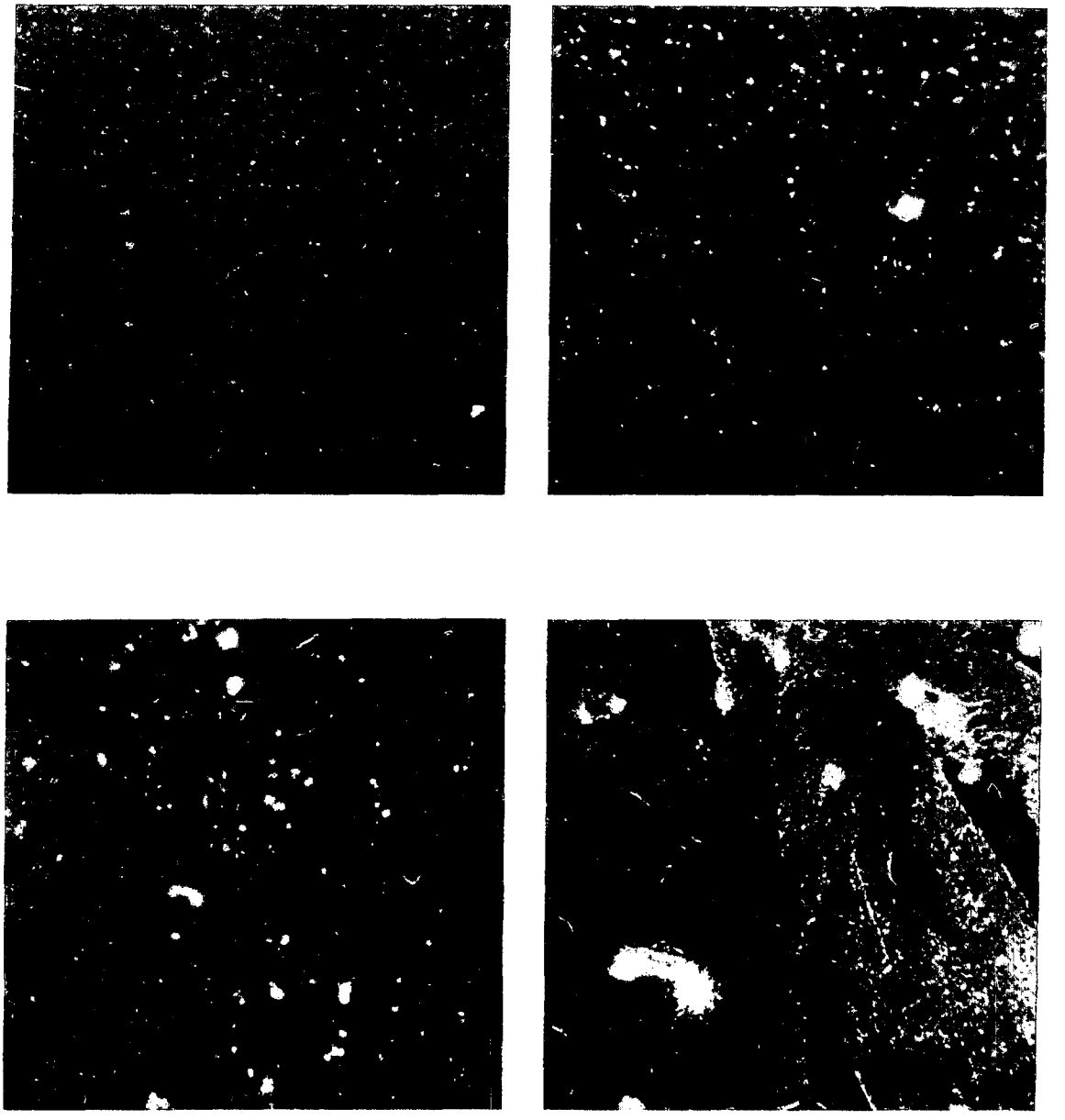

Fig. 53. Microstructure of TaC-C composite containing 5 wt% 1.3 μm TaC-30. (Scanning electron micrographs. Top left, 100X. Top right, 300X. Bottom left, 1000X. Bottom right, 3000X.)

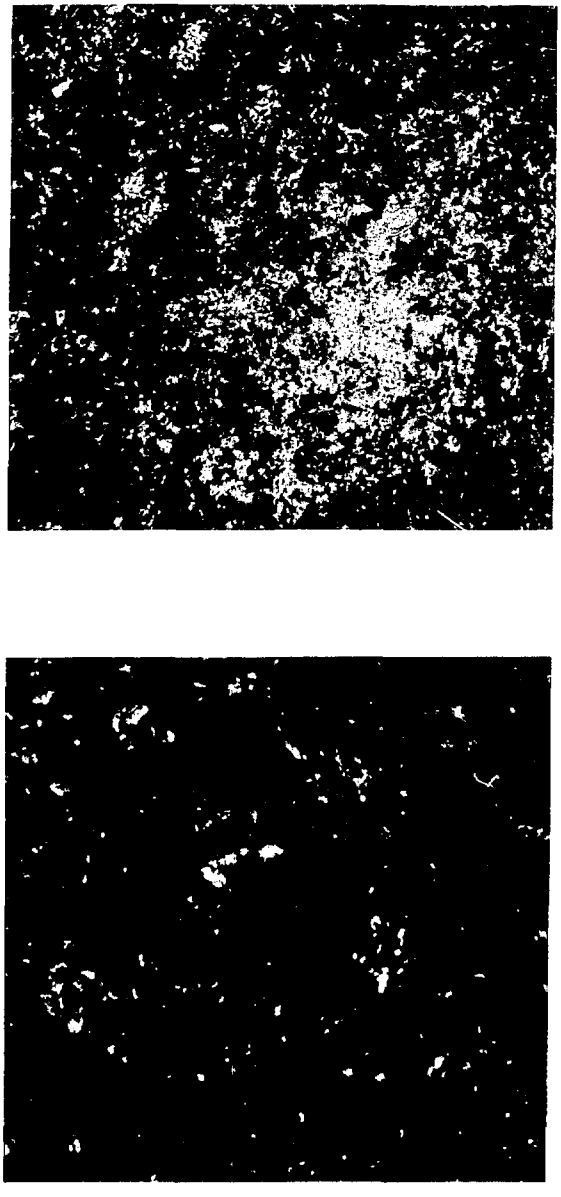

Fig. 54. Microstructure of TaC-C composite containing 7 wt% 1.3 μm TaC-30. (Conventional metallography. Top, 100X. Bottom, 500X.)

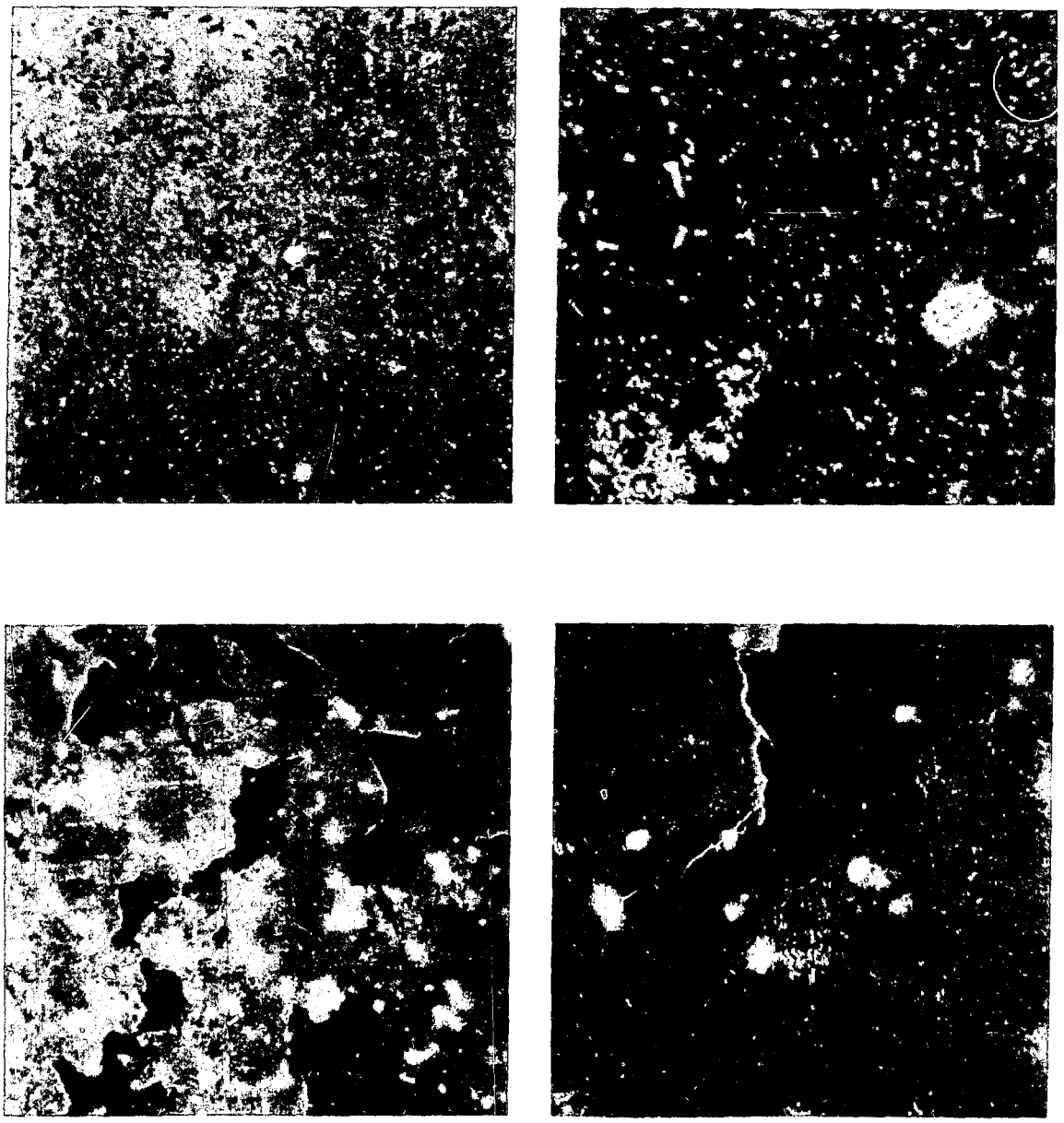

Fig. 55. Microstructure of TaC-C composite containing 7 wt% 1.3 μm TaC-30. (Scanning electron micrographs. Top left, 100X. Top right, 300X. Bottom left, 1000X. Bottom right, 3000X.)

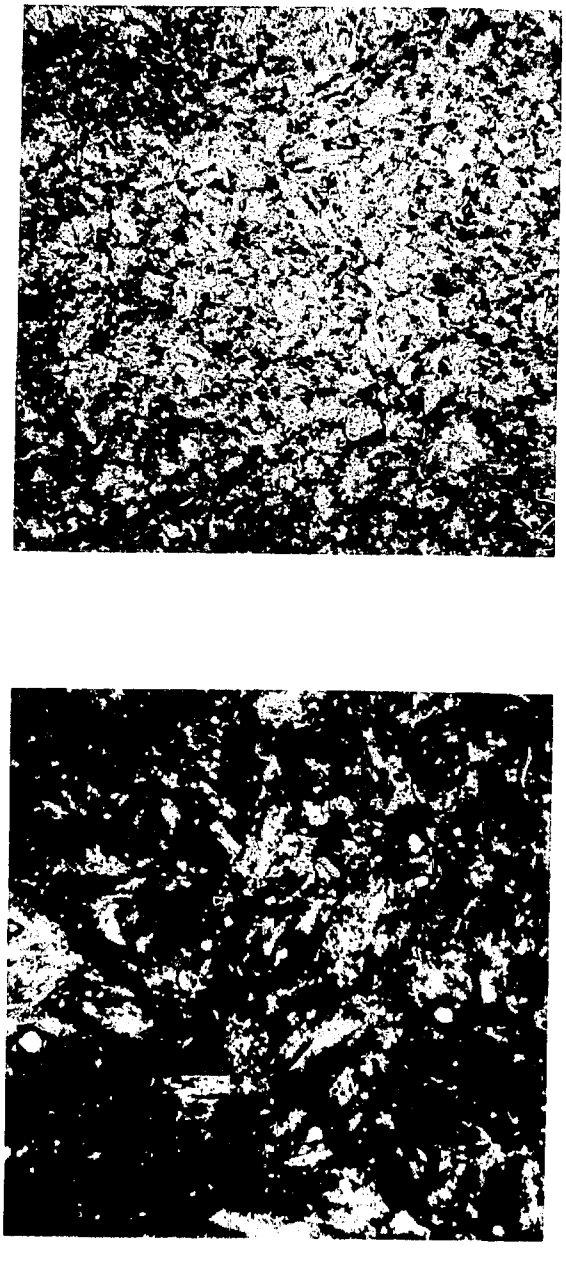

Fig. 56. Microstructure of TaC-C composite containing 14 wt% 1.3 μm TaC-30. (Conventional metallography. Top, 100X. Bottom, 500X.)

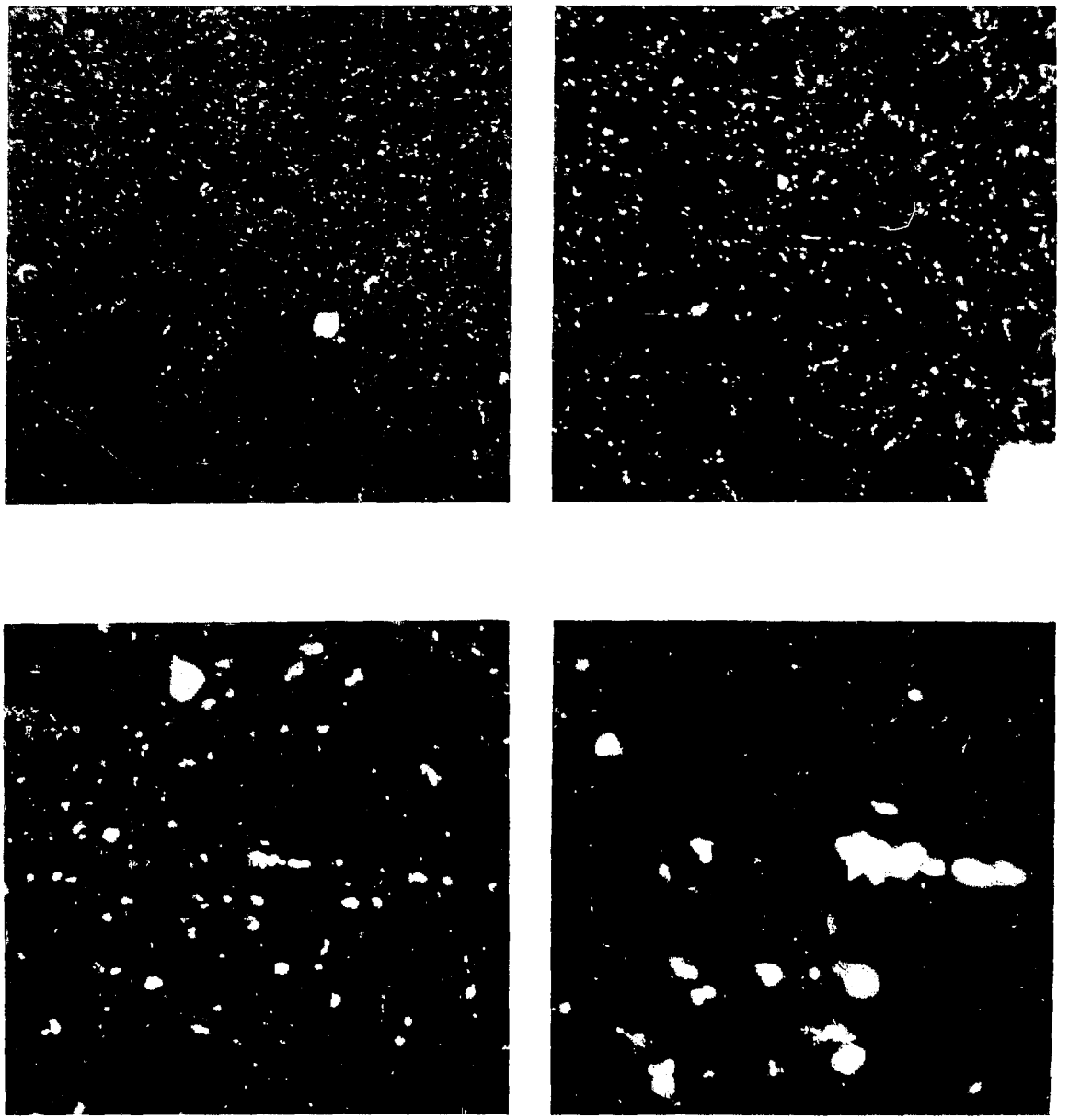

Fig. 57. Microstructure of TaC-C composite containing 14 wt% 1.3 μm TaC-30. (Scanning electron micrographs. Top left, 100X. Top right, 300X. Bottom left, 1000X. Bottom right, 3000X.)

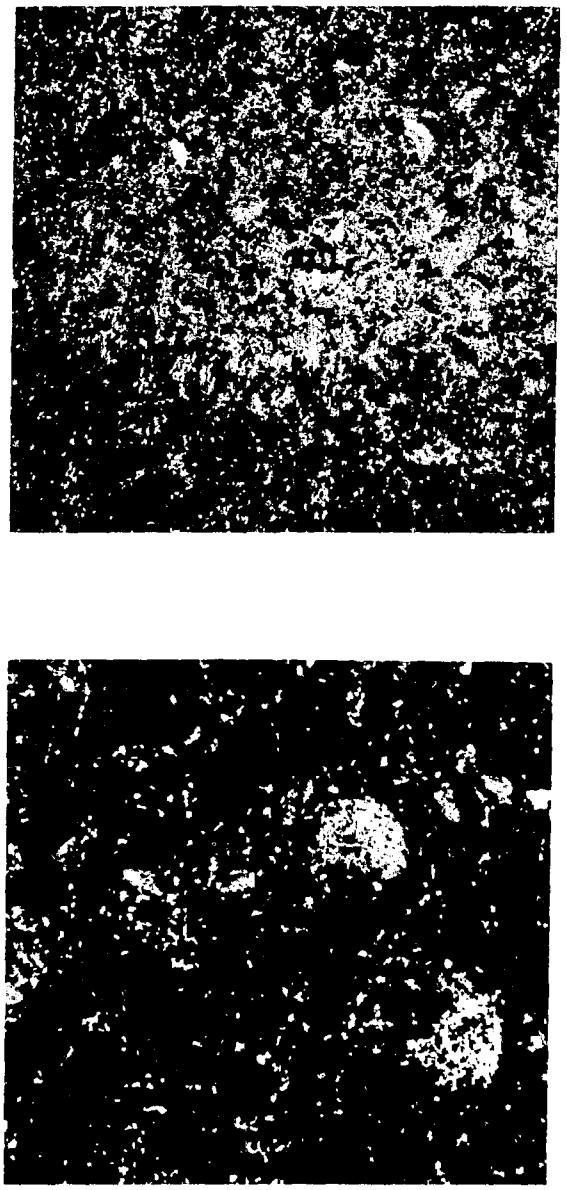

Fig. 58. Microstructure of TaC-C composite containing 40 wt% 1.3 μm TaC-30. (Conventional metallography. Top, 100X. Bottom, 500X.)

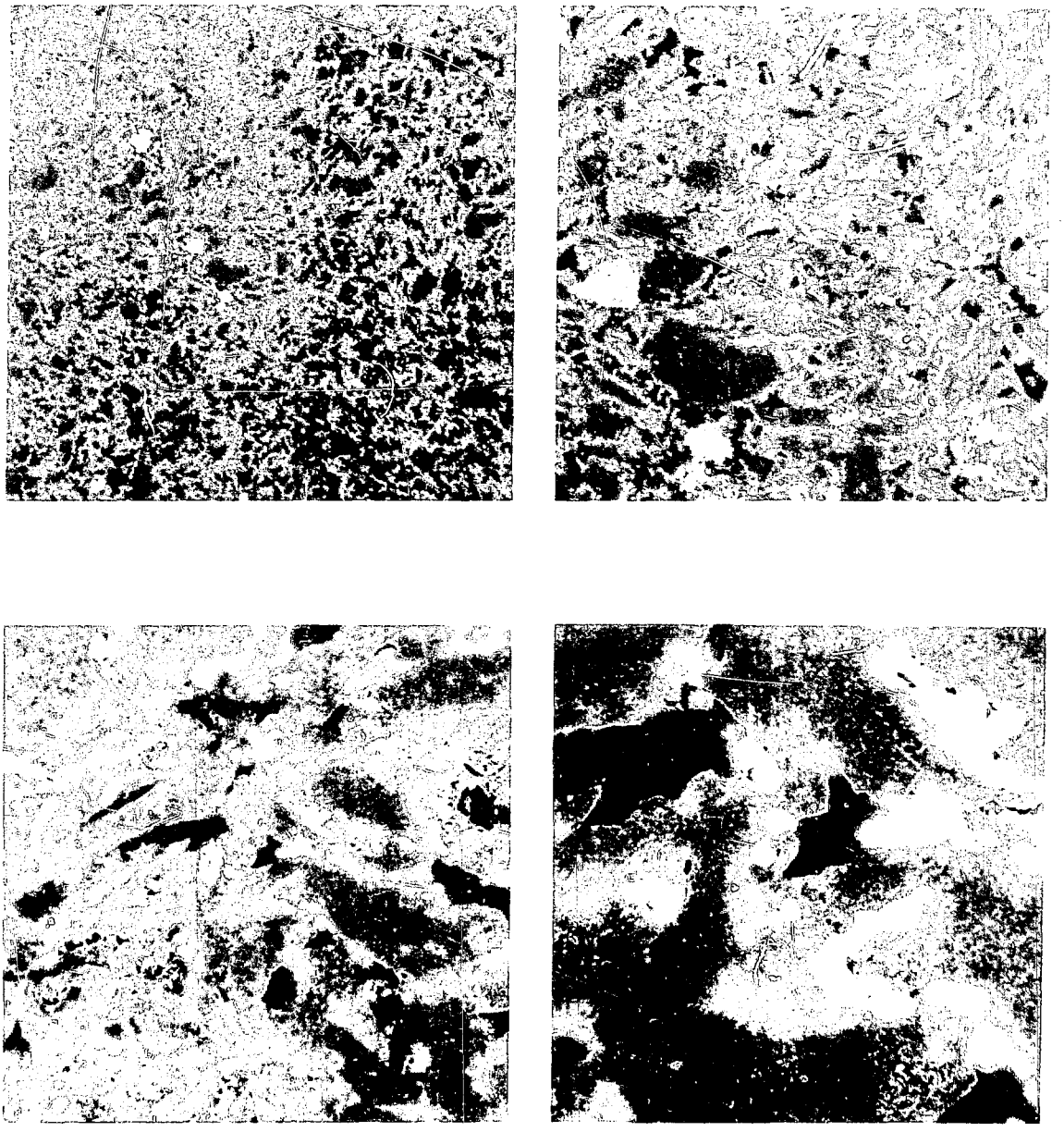

Fig. 59. Microstructure of TaC-C composite containing 40 wt% 1.3 μm TaC-30. (Scanning electron micrographs. Top left, 100X. Top right, 300X. Bottom left, 1000X. Bottom right, 3000X.)

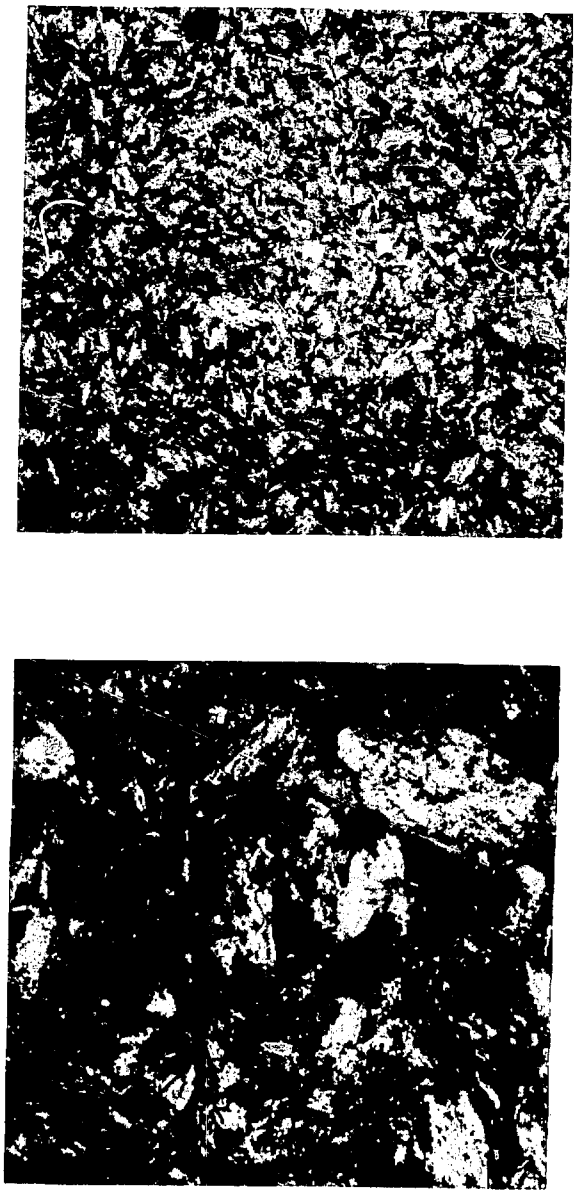

Fig. 60. Microstructure of TaC-C composite containing 1 wt% 40 μm TaC-45. (Conventional metallography. Top, 100X. Bottom, 500X.)

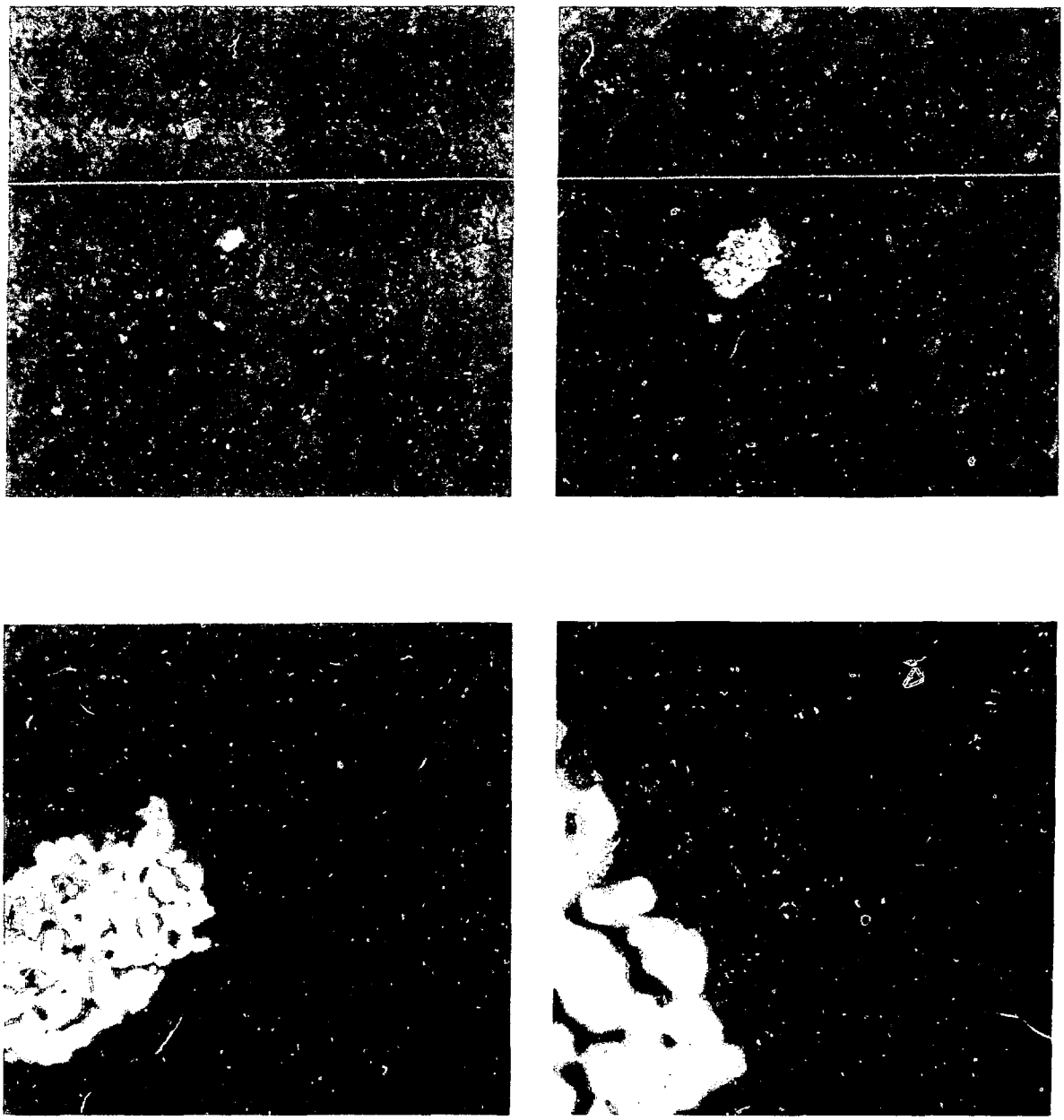

Fig. 61. Microstructure of TaC-C composite containing 1 wt% nominal 40 μm TaC-45. (Scanning electron micrographs. Top left, 100X. Top right, 300X. Bottom left, 1000X. Bottom right, 3000X.)

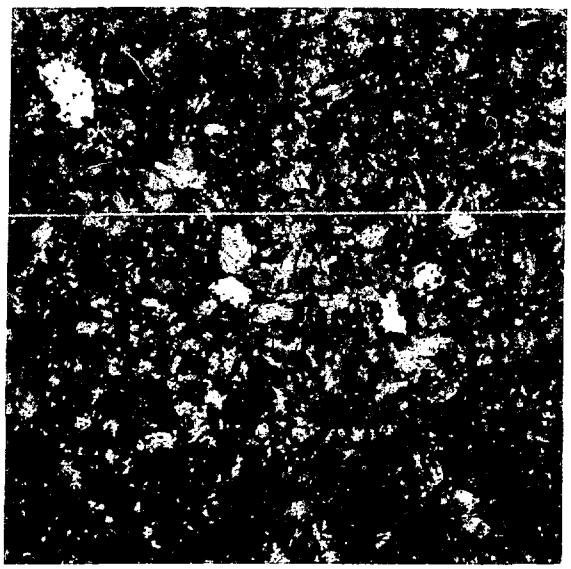

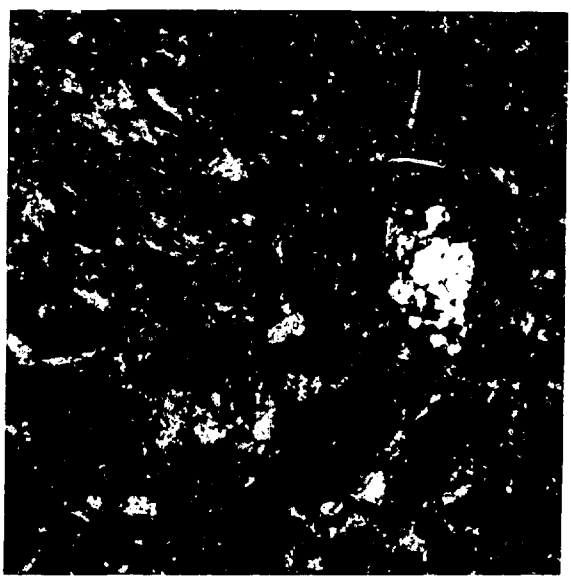

Fig. 62. Microstructure of TaC-C composite containing 5 wt% 40 μm TaC-45. (Conventional metallography. Top, 100X. Bottom, 500X.)

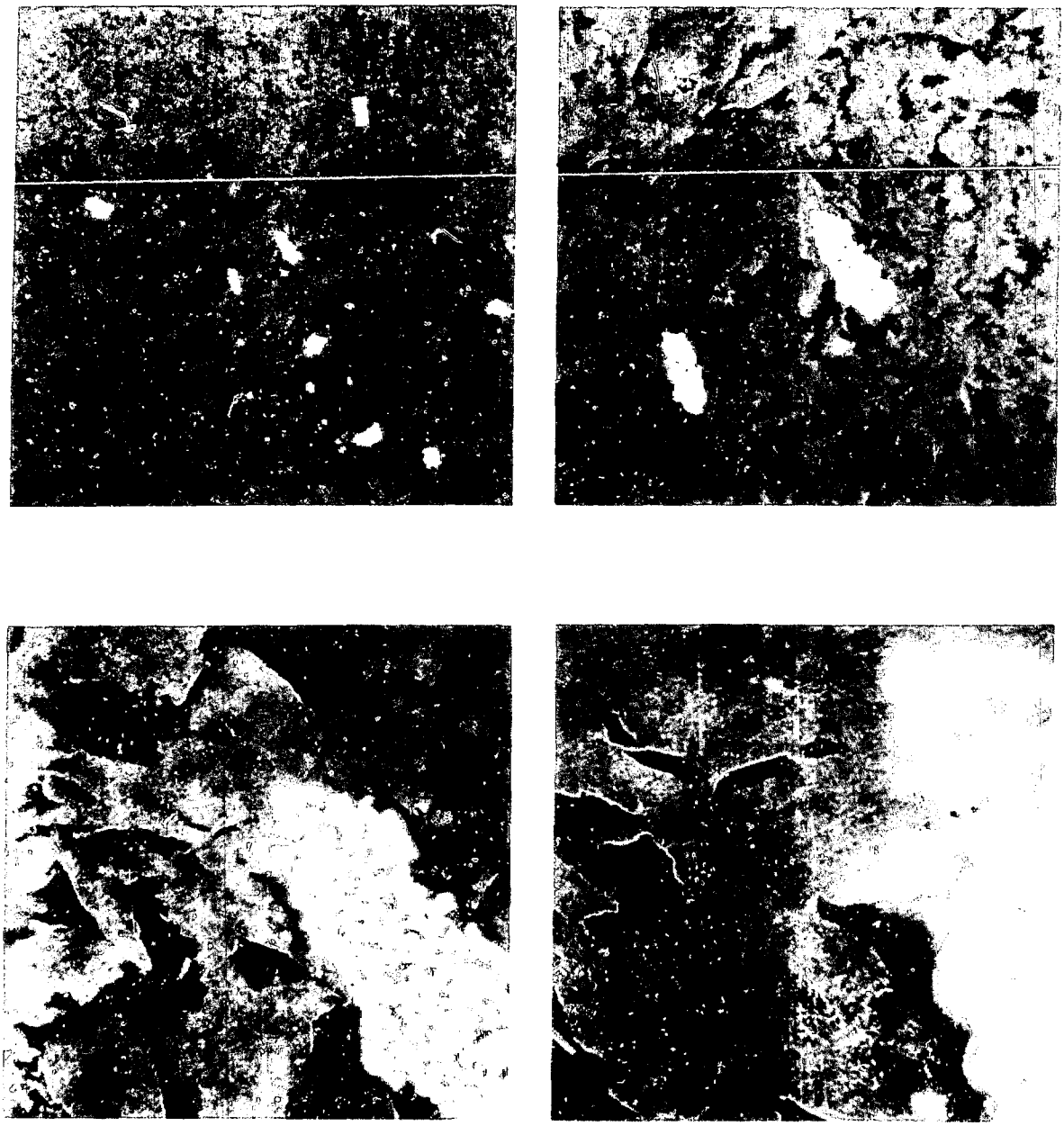

Fig. 63. Microstructure of TaC-C composite containing 5 wt% nominal 40 μm TaC-45. (Scanning electron micrographs. Top left, 100X. Top right, 300X. Bottom left, 1000X. Bottom right, 3000X.)

Fig. 64. Microstructure of TaC-C composite containing 7 wt% 40 μm TaC-45. (Conventional metallography. Top, 100X. Bottom, 500X.)

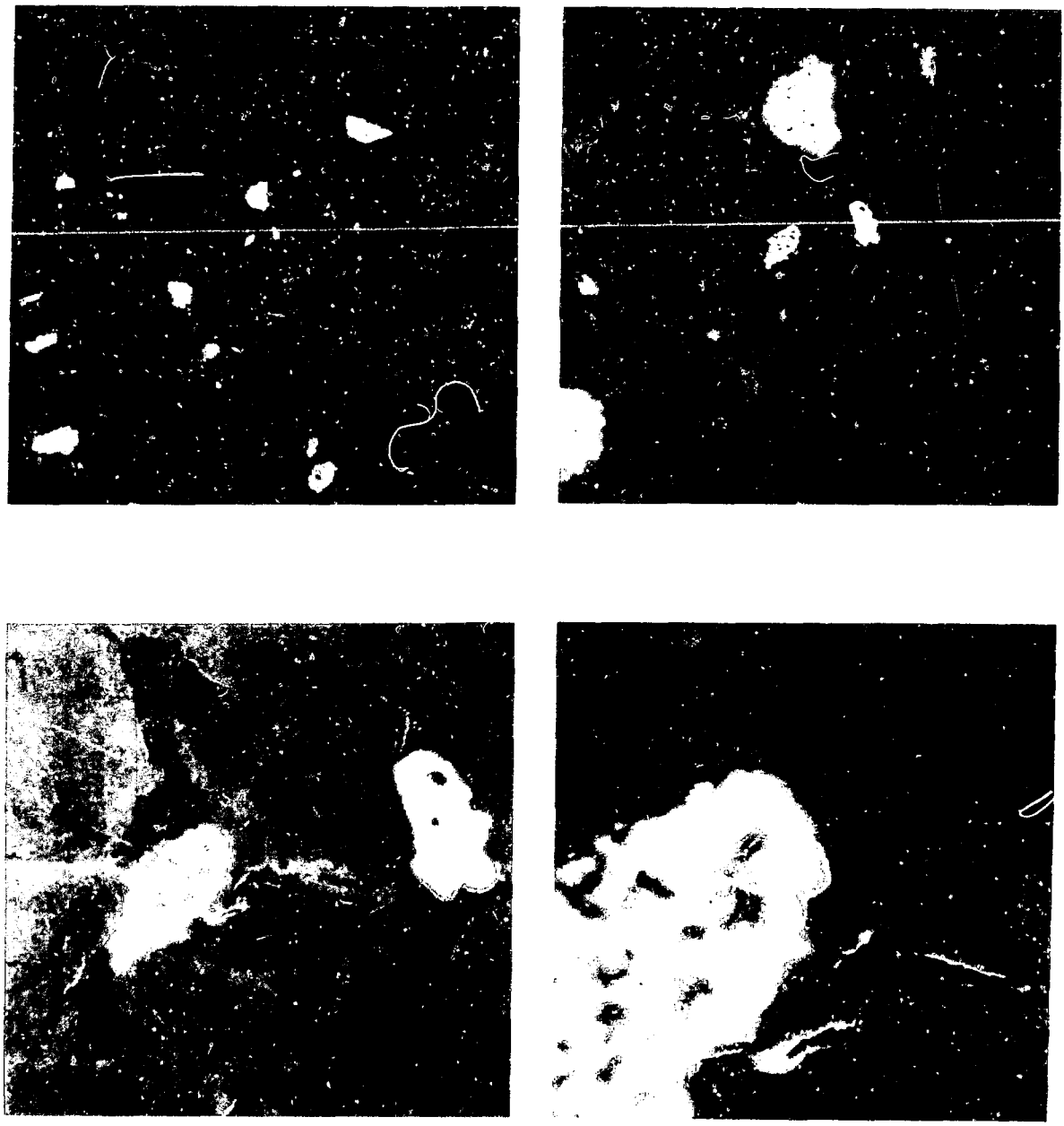

Fig. 65. Microstructure of TaC-C composite containing 7 wt% nominal 40 μm TaC-45. (Scanning electron micrographs. Top left, 100X. Top right, 300X. Bottom left, 1000X. Bottom right, 3000X.)

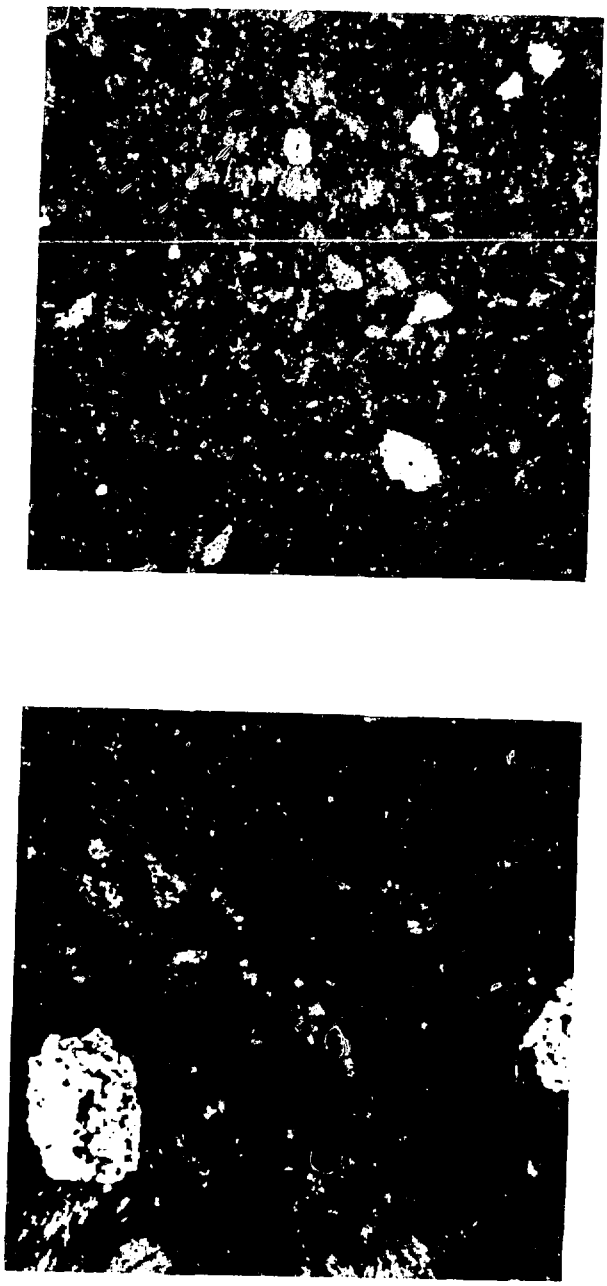

Fig. 66. Microstructure of TaC-C composite containing 14 wt% 40 μm TaC-45. (Conventional metallography. Top, 100X. Bottom, 500X.)

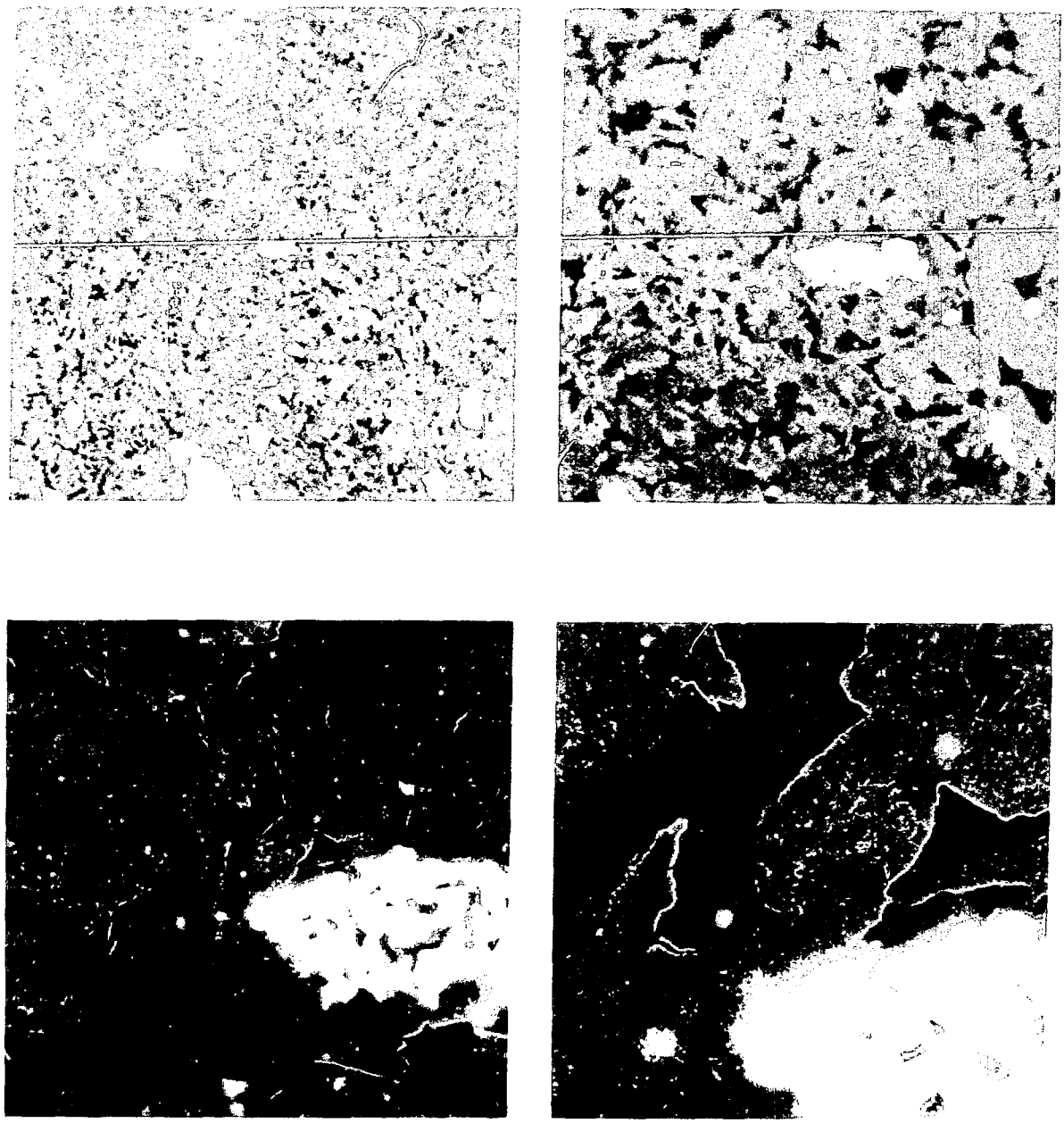

Fig. 67. Microstructure of TaC-C composite containing 14 wt% nominal 40 μm TaC-45. (Scanning electron micrographs. Top left, 100X. Top right, 300X. Bottom left, 1000X. Bottom right, 3000X.)

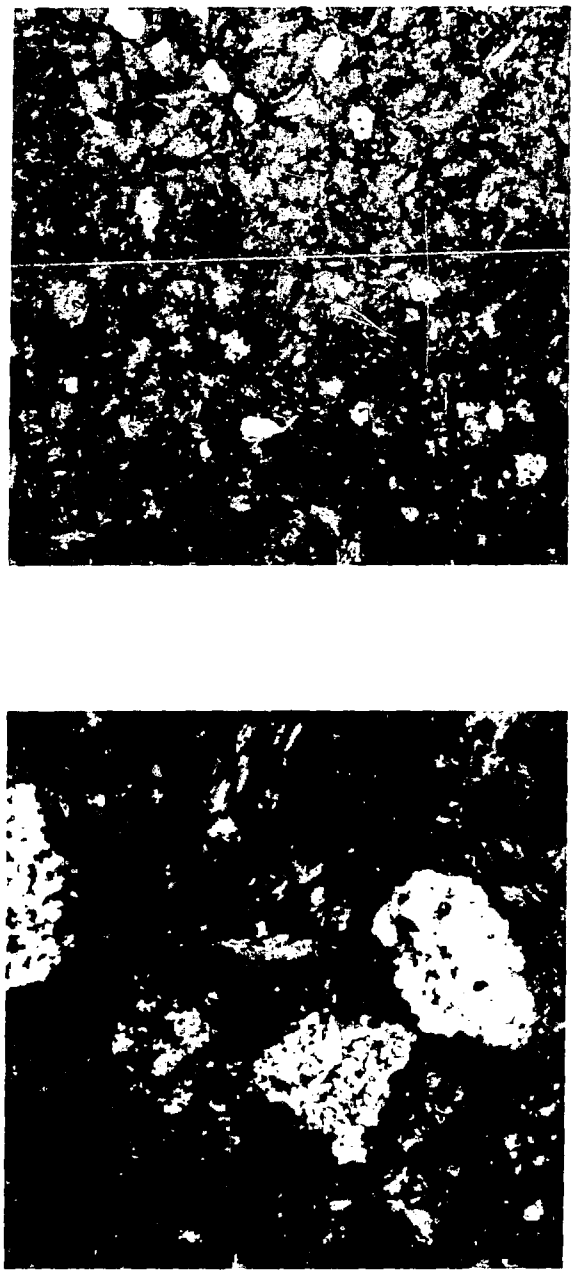

Fig. 68. Microstructure of TaC-C composite containing 20 wt% 40 μm TaC-45. (Conventional metallography. Top, 100X. Bottom, 500X.)

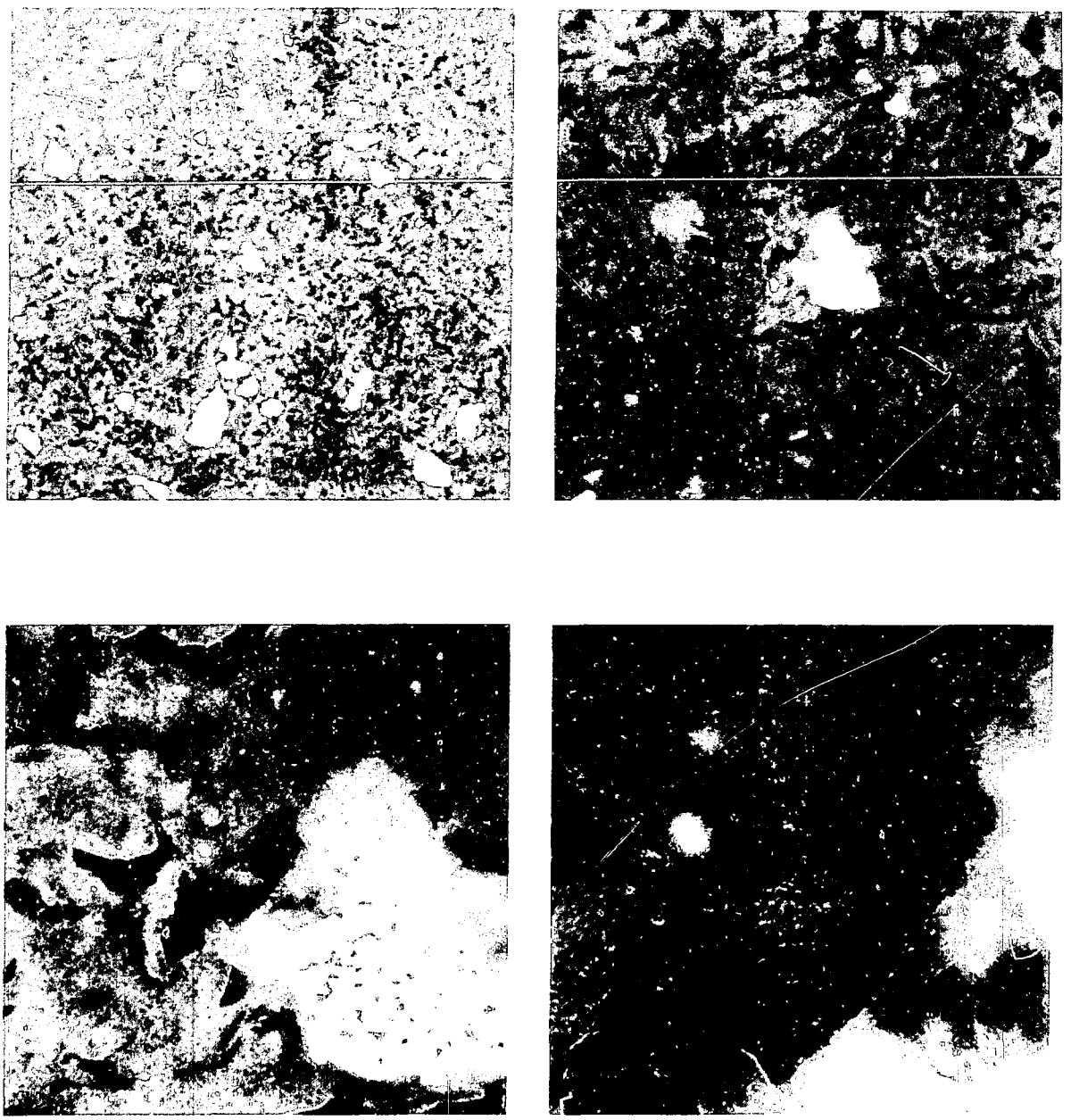

Fig. 69. Microstructure of TaC-C composite containing 20 wt% nominal 40 μm TaC-45. (Scanning electron micrographs. Top left, 100X. Top right, 300X. Bottom left, 1000X. Bottom right, 3000X.)

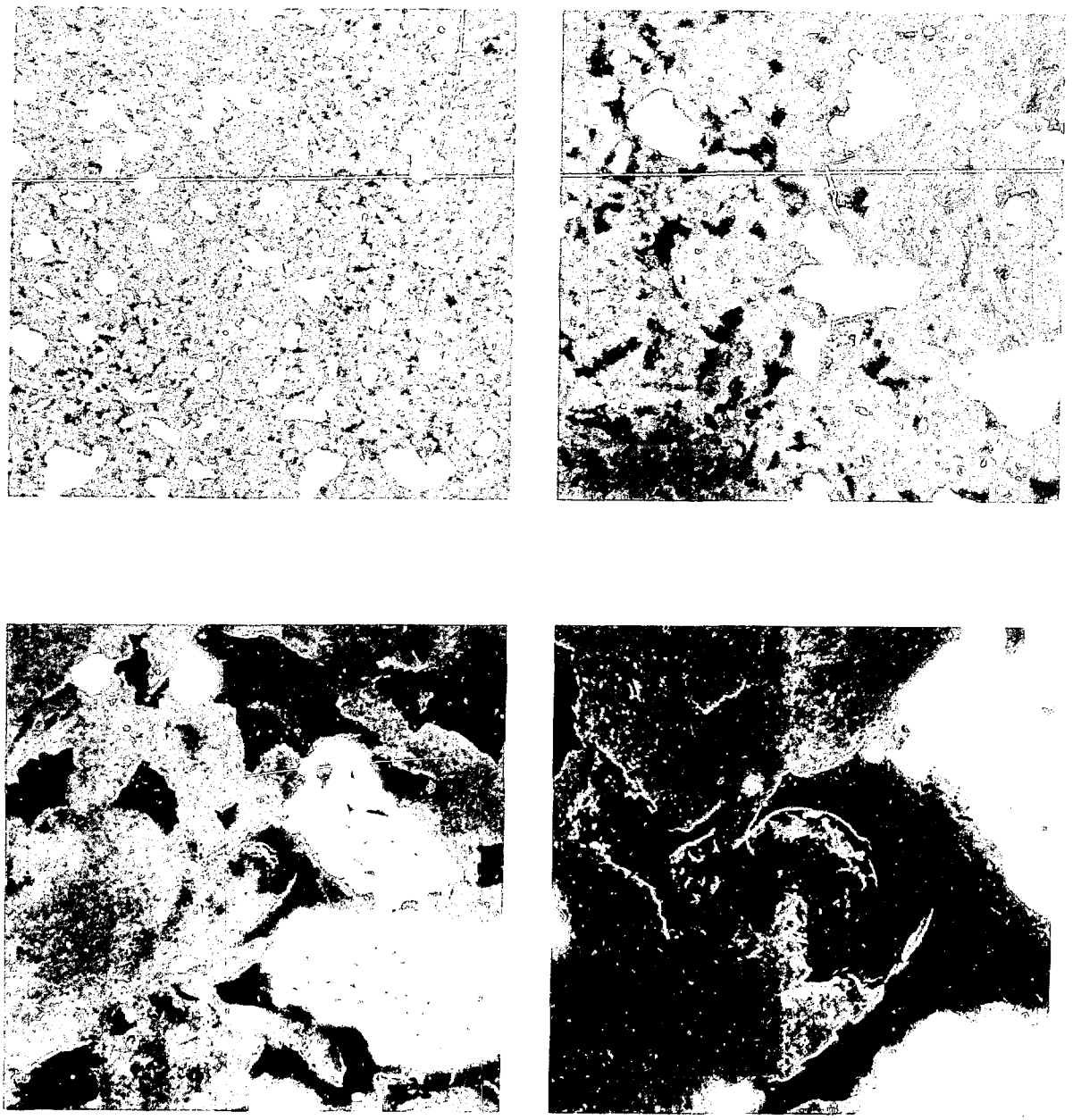

Fig. 7C. Microstructure of TaC-C composite containing 40 wt% nominal 40 μm TaC-45. (Scanning electron micrographs. Top left, 100X. Top right, 300X. Bottom left, 1000X. Bottom right, 3000X.)

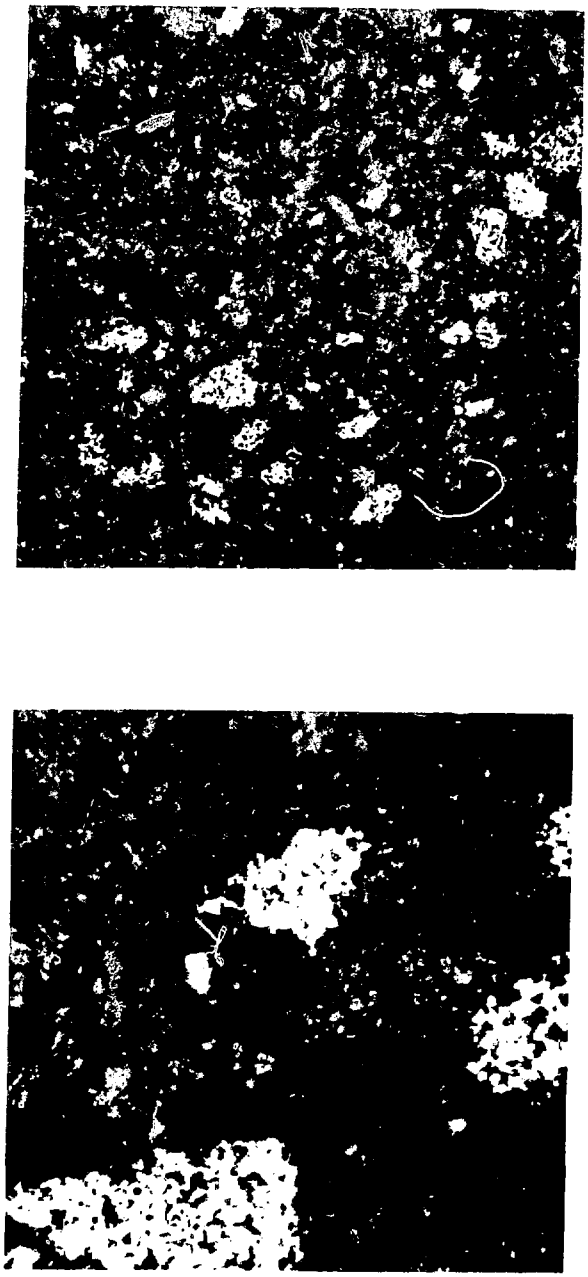

Fig. 71. Microstructure of TaC-C composite containing 40 wt% 40 μm TaC-45. (Conventional metallography. Top, 100X. Bottom, 500X.)

ALT:486(260)

☆ US GOVERNMENT PRINTING OFFICE: 1973—784-277/15